Neurobiology of Disease 174 (2022) 105896

Contents lists available at ScienceDirect

Neurobiology of Disease

journal homepage: www.elsevier.com/locate/ynbdi

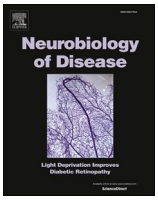

A CRISPR/Cas9-engineered avatar mouse model of monocarboxylate transporter 8 deficiency displays distinct neurological alterations

Víctor Valcárcel-Hernández [a], Marina Guillén-Yunta [a,1], Miranda Bueno-Arribas [b,1], Ana Montero-Pedrazuela [a], Carmen Grijota-Martínez [a,c], Suzy Markossian [d], Ángel García-Aldea [a], Frédéric Flamant [d], Soledad Bárez-López [a,e,*], Ana Guadaño-Ferraz [a,**]

[a] Department of Endocrine and Nervous System Pathophysiology, Instituto de Investigaciones Biomédicas Alberto Sols, Consejo Superior de Investigaciones Científicas (CSIC)-Universidad Autónoma de Madrid (UAM), Madrid, Spain
[b] Department of Experimental Models of Human Diseases, Instituto de Investigaciones Biomédicas Alberto Sols, Consejo Superior de Investigaciones Científicas (CSIC)-Universidad Autónoma de Madrid (UAM), Madrid, Spain
[c] Department of Cell Biology, Faculty of Biology, Universidad Complutense de Madrid, Madrid, Spain
[d] Institut de Genomique Fonctionnelle de Lyon, INRAE USC1370, CNRS UMR 5242, Ecole Normale Superieure de Lyon, Universite Claude Bernard Lyon 1, Lyon, France
[e] Translational Health Sciences, Bristol Medical School, University of Bristol, Bristol, United Kingdom

ARTICLE INFO

Keywords:
Thyroid hormones
Thyroid hormone transport
MCT8
Murine model
GABAergic system
CRISPR/Cas9

ABSTRACT

Inactivating mutations in the specific thyroid hormone transporter monocarboxylate transporter 8 (MCT8) lead to an X-linked rare disease named MCT8 deficiency or Allan-Herndon-Dudley Syndrome. Patients exhibit a plethora of severe endocrine and neurological alterations, with no effective treatment for the neurological symptoms. An optimal mammalian model is essential to explore the pathological mechanisms and potential therapeutic approaches. Here we have generated by CRISPR/Cas9 an avatar mouse model for MCT8 deficiency with a point mutation found in two MCT8-deficient patients (P253L mice). We have predicted by *in silico* studies that this mutation alters the substrate binding pocket being the probable cause for impairing thyroid hormone transport. We have characterized the phenotype of MCT8-P253L mice and found endocrine alterations similar to those described in patients and in MCT8-deficient mice. Importantly, we detected brain hypothyroidism, structural and functional neurological alterations resembling the patient's neurological impairments. Thus, the P253L mouse provides a valuable model for studying the pathophysiology of MCT8 deficiency and in the future will allow to test therapeutic alternatives such as *in vivo* gene therapy and pharmacological chaperone therapy to improve the neurological impairments in MCT8 deficiency.

1. Introduction

Mutations in the monocarboxylate transporter 8 (MCT8) encoded by the *SLC16A2* gene, lead to the X-linked rare disease known as Allan-Herndon-Dudley syndrome (AHDS) or MCT8 deficiency in males (Allan et al., 1944; Dumitrescu et al., 2004; Friesema et al., 2004). MCT8 is a thyroid hormone (TH)-specific cell membrane transporter (Friesema et al., 2003) with a crucial role in TH availability and action, especially during central nervous system (CNS) development (Bernal et al., 2015; López-Espíndola et al., 2014; Refetoff et al., 2021). Patients diagnosed with AHDS are characterized by altered serum levels of THs with high serum concentrations of triiodothyronine (T3), low thyroxine (T4) and reverse triiodothyronine (rT3), and normal to slightly high levels of the thyroid stimulating hormone (TSH) (Dumitrescu et al., 2004; Friesema et al., 2004). In contrast, the brain exhibits signs of hypothyroidism (López-Espíndola et al., 2014), resulting in severe psychomotor impairments and global developmental delay along with profound intellectual disability (IQ < 30) and speech difficulties. AHDS is also related to central hypotonia, spastic paraplegia and dystonic movements (Dumitrescu et al., 2004; Friesema et al., 2004; Masnada et al., 2022; Matheus et al., 2015; Sarret et al., 2022; Schwartz and Stevenson, 2007). Given its atypical clinical features, associating brain hypothyroidism

* Correspondence to: S B-López, Bristol Medical School, University of Bristol, Dorothy Hodgkin Building, Whitson Street, Bristol BS1 3NY, United Kingdom.
** Correspondence to: A G-Ferraz, Instituto de Investigaciones Biomédicas, CSIC-UAM, Arturo Duperier 4, 28029 Madrid, Spain.
E-mail addresses: ze18625@bristol.ac.uk (S. Bárez-López), ana.guadano.ferraz@csic.es (A. Guadaño-Ferraz).
[1] MG-Y and MB-A contributed equally to this work.

https://doi.org/10.1016/j.nbd.2022.105896
Received 2 June 2022; Received in revised form 30 September 2022; Accepted 11 October 2022
Available online 13 October 2022

and peripheral hyperthyroidism, treatment options for MCT8-deficient patients are very limited (Grijota-Martínez et al., 2020).

There are currently >100 known mutations of *SLC16A2*. Three subtypes can be distinguished: Type 1 mutations where the transport capacity of the protein is partially (type 1A) or completely (type 1B) compromised. Type 2 mutations reduce the presence of the protein at the plasma membrane, but do not eliminate its transport activity. Type 3 mutations include large deletions and frameshift mutations that fully inactivate protein function (Groeneweg et al., 2019b). The P321L missense mutation is representative of type 1B mutations, which are associated with very severe neurological symptoms, but could be amenable to pharmacological treatment, favoring the restoration of transport activity (Braun et al., 2022; Kersseboom et al., 2013). It was discovered in twin brothers and inherited from a healthy heterozygous mother (Vaurs-Barrière et al., 2009; Verge et al., 2012).

Slc16a2 KO (*Mct8* KO) mice were firstly generated as a model for AHDS. Although these mice faithfully replicate the alterations in the circulating THs concentrations of patients (Dumitrescu et al., 2006; Trajkovic et al., 2007) their use as a model for AHDS has two limitations. First, they are only relevant to type 3 mutations, and cannot be used to test the pharmacological interventions mentioned above. Second, their neurodevelopment is only marginally altered, and they do not reproduce the neurological abnormalities observed in patients (Wirth et al., 2009). This surprising absence of neurological defects is currently interpreted as resulting from a compensatory mechanism in mice involving the transport of T4 through the Organic Anion Transporter 1C1 (OATP1C1) across the brain barriers and the local conversion of T4 into T3 by the enzyme deiodinase 2 (DIO2) on the astrocytes (Bárez-López et al., 2017b; Ceballos et al., 2009; Morte et al., 2010a; Wirth et al., 2009). For that reason, the double mutant mice *Mct8/Oatp1c1* KO and *Mct8/Dio2* KO display neurodevelopmental defects not observed in single KO mice (Bárez-López et al., 2019; Mayerl et al., 2014). Even though both models mimic human MCT8 deficiency, they present some limitations. For instance, OATP1C1 transports other compounds in addition to T4, including steroid hormone metabolites (Westholm et al., 2009), therefore the phenotypic outcome of *Mct8/Oatp1c1* KO animals could also be due to alterations in the transport of other molecules. Moreover, a mutation in the OATP1C1 transporter *SLCO1C1* gene in humans has been reported to be linked with brain hypometabolism, brain-specific hypothyroidism, and juvenile neurodegeneration (Strømme et al., 2018). Even though the phenotypic outcome of *Mct8/Dio2* KO mice is solely due to impaired THs action, this model also presents some limitations as increased DIO2 activity is a compensatory mechanism in MCT8 deficient patients (López-Espíndola et al., 2014). For all these issues, additional models of the syndrome targeting MCT8 alone, but reproducing its neurological alterations more faithfully than the *Mct8* KO model, would contribute to the understanding of the mechanisms that underlie MCT8 deficiency more accurately.

We present here a novel mouse model with the MCT8-P253L mutation, equivalent to the human P321L missense mutation (P253L mice) (Teixeira et al., 2018; Vaurs-Barrière et al., 2009). These mice provide a unique opportunity to explore the consequences of the P253L substitution, instead of deleting MCT8 alone or inactivating both MCT8 and OATP1C1 or DIO2. First, we performed *in silico* predictions of the tertiary structure of the mutant protein that have shown important alterations in the pocket size and the TH binding site accessibility in the P321L mutated protein. Then, the mutation was introduced by homologous recombination in the mouse genome, using CRISPR/Cas9 genome editing. Comparing P253L mice with wild-type mice and the classic *Mct8* KO model we have found that, as *Mct8* KO mice, P253L mice exhibited an endocrine phenotype similar to AHDS patients with peripheral hyperthyroidism and brain hypothyroidism. Interestingly, in contrast to *Mct8* KO mice, P253L animals exhibited several neurological alterations, ranging from impairments on the whole neuroarchitecture to alterations affecting particularly the GABAergic system. All these endocrine and histopathological traits derived in a late-onset motor and emotional phenotype with motor skills alterations and anxiety-like behavior. Based on our findings, we propose that the P253L avatar mouse represents a new suitable animal model for studying human MCT8 deficiency and a valuable tool for testing therapeutic interventions including gene repair and chaperone therapy approaches.

2. Methods

2.1. In silico analyses

2.1.1. Gene alignment

Some of the available MCT8 orthologues and all human MCT family members were aligned to analyze shared and divergent features in amino acid composition. All amino acid sequence alignments were created automatically by means of Clustal Omega (Sievers and Higgins, 2018) software applying the Blossum62 amino acid similarity matrix. Alignments were produced with the BioEdit software package.

The potential dimensions of transmembrane helices (TMHs) were predicted based on observable helices in the crystal structure of MCT1 (PDB code 6LYY (Wang et al., 2021)), which was ultimately used as a structural template for homology models (see protein structure prediction).

2.1.2. Protein structure prediction

The crystal structure of the outward-facing conformation of human MCT1 (PDB 6LYY), was used as a template to model the structure for the short sequence of MCT8 and MCT8-P321L (as named after the sequence on the long isoform) (Wang et al., 2021), by means of Robetta server (Baek et al., 2021). The alignment between human MCT8 and MCT1 amino acid sequences reveals a similarity score of 35.73% (Supplemental Fig. 1). With little-to-no deviations, MCT1 TMHs are applicable for human MCT8. The two models with better score in the Robetta server were selected and refined to eliminate non-precisely predicted residues (>5 Å of error). The reliability of both structural templates was then validated with VERIFY3D, PROCHECK, and ERRAT2 and servers (Bowie et al., 1991; Colovos and Yeates, 1993; Laskowski et al., 1996). MCT8 and MCT8-P321L obtained a great score in all three servers: 83.53% and 87.69% 3D—1D score in VERIFY3D (where >80% is optimal), 94.76% and 94.1% of the residues in most favored regions (where >90 is optimal) as assessed by PROCHECK and an overall quality factor of 96.99 and 99.86 (where >90 is optimal) in ERRAT2, respectively. Two artificial MCT8 mutants (P462L and K207L) were also modeled as a control, to validate the accuracy of the *in silico* approach in assessing the structural changes of the disease-causing mutation.

PyMOL software (PyMOL Molecular Graphics System, V. 2.4.0 Schrödinger, LLC) was used for the visualization and analysis of the models. The intra-protein interactions changes between MCT8 and MCT8-P321L models were assessed by generating a residue interaction network, using the RING 2.0 web server (Martin et al., 2011; Piovesan et al., 2016). CASTp server and PyMOL were used for substrate-binding pocket volume analysis (Tian et al., 2018).

We then used the structure comparison program FATCAT (Flexible structure AlignmenT by Chaining Aligned fragment pairs allowing Twists) (Li et al., 2020; Ye and Godzik, 2003) to compare the structure of short human MCT8 isoform we had generated with Robetta with the recently published predicted structure of this protein generated by the newly released AlphaFold software (Tunyasuvunakool et al., 2021). FATCAT showed that both structures are significatively similar (*p*-value 4.48 e-12; 83.64% identity), and differences are located in the poorly predicted N-terminal region (Supplemental Fig. 2F, G).

2.2. Animal models

Animals were housed in light- and temperature-controlled conditions at 22 ± 2 °C on a 12:12 light-dark cycle (lights on at 7 AM), with *ad libitum* food and water access. In all experiments, wild-type (WT), P253L

and *Mct8* KO male mice were used, as AHDS is an X-linked disease and thus, only affects males. The generation of P253L mice by electroporation of mouse oocytes, using a single stranded oligonucleotide as template, was reported previously (Teixeira et al., 2018). Founder mice were backcrossed for at least 6 generations with C57Bl6/J wild-type mice to segregate putative off-target mutations and ensure a homogenous genetic background. For the obtention of the studied animals, male WT mice are crossed with heterozygous females and then screened by PCR as described in Teixeira et al. (2018) Genotypes were confirmed by PCR of ear DNA (25 cycles at 58 °C annealing temperature) using the following primers: forward common, 5′GGTGCATTCTCACTCT GAGTTCC3′; reverse common, 5′ GCAGACAGAGCTGATTTCCTAT GTG3′; forward specific for the mutation, 5′AGGTTGGTGGCGAGTGT GG3′; reverse specific for the mutation 5′TATCCCCCAGCATTTT AATTAAAAAC3′. Using this procedure all samples generated a 100-bp PCR product and the mutated alleles a 309-bp product. *Mct8* KO genotype was confirmed by ear DNA PCR as described in Ceballos et al. (2009). WT mice used for every experiment included both P253L and *Mct8* KO littermates. TH determinations and gene expression analyses were performed at 3 months of age (P90). Histological analyses, motor task assessments and behavioral tasks were done at 3 and 6 (P180) months of age. Hearing assessment and audiogenic seizure assays were performed in P90 mice.

For histological procedures mice ($n = 4$) were anesthetized with ketamine (75 μg/g of body weight) and medetomidine hydrochloride (1 μg/g of body weight), and transcardially perfused with 4% paraformaldehyde in 0.1 M phosphate buffer (PB). Brains were removed, post-fixed overnight in 4% paraformaldehyde in 0.1 M PB, cryoprotected with 30% sucrose and cut into 30 μm free-floating sections on a cryostat.

For hormonal determinations in plasma and tissues ($n = 10$) and gene expression assays ($n = 8$), mice were anesthetized as above and transcardially perfused with saline to remove blood from tissues before their collection. Before perfusion, blood was extracted by retroorbital collection and used for the determination of T4 and T3 plasma concentrations. Tissues (cerebral cortex, cerebellum and liver) were harvested and preserved at −80 °C until RNA extraction or hormonal determination.

Mice were studied at P90 and P180, as these young-adult and adult timepoints have been extensively studied in other models of MCT8 deficiency and other models with impairments in thyroid hormone signaling (Bárez-López et al., 2017a, 2019; Venero et al., 2005).

2.3. Hormonal determinations in plasma and tissues

High specific activity ^{125}I-T3 and ^{125}I-T4 (3000 μCi/μg) were obtained by labeling (3, 5)-T2 (D0629; Sigma) and T3 (T2877; Sigma) as substrates with ^{125}I (NEZ033A; Perkin Elmer), as previously described (Obregon et al., 1978; Weeke and Örskov, 1973). One minor modification was the separation of the labeled products, which was done by ascending paper chromatography for 16 h in presence of butanol–ethanol–ammonia 0.5 N (5:1:2) as solvent. The ^{125}I-T3 and ^{125}I-T4 were eluted and kept in ethanol at 4 °C. T3 and T4 were extracted from individual 80 μL aliquots of plasma with methanol (1:6), evaporated to dryness and taken up in the radioimmunoassay buffer for determinations. T3 and T4 extraction from tissues (cerebral cortex, liver and cerebellum), as well as determinations of T3 and T4, were performed as previously described (Morreale de Escobar et al., 1985; Ruiz de Oña et al., 1988) with the dynamic range being 0.4–100 pg T3/tube and 2.5–320 pg T4/tube.

2.4. Gene expression

RNA was isolated from individual hemi brain cortex. Total RNA was extracted using TRIZOL reagent (Invitrogen; 15596026) following the manufacturer's recommendations with an additional chloroform extraction. cDNA was prepared from 250 ng of RNA using the high-capacity cDNA reverse transcription kit (Applied Biosystems). A cDNA aliquot corresponding to 5 ng of the starting RNA was used. Real-time PCR was performed with the TaqMan universal PCR master mix, No Amp Erase UNG (Applied Biosystems) on a 7900HT fast real-time PCR system (Applied Biosystems). The PCR program consisted of a hot start of 95 °C for 10 min, followed by 40 cycles of 15 s at 95 °C and one min at 60 °C. PCRs were performed in triplicate using the *18S* gene as internal standard and the two-cycle threshold method for analysis. The expression of the following T3-dependent genes was measured using Applied Biosystems TaqMan probes: *Dio2* (type 2 deiodinase, Mm00515664_m1), *Dio3* (type 3 deiodinase, Mm00548953_s1), *Cbr2* (carbonyl reductase 2, Mm00483074_g1), *Cntn2* (contactin 2, Mm00516138_m1), *Flywch2* (Flywch family member 2, Mm00513052_m1), *Hr* (hairless, Mm00498963_m1), *Mbp* (Myelin basic protein, Mm01266402_m1), and *Nefm* (neurofilament, medium polypeptide, Mm00456201_m1), *Slco1c1* or *Oatp1c1* (Solute carrier organic anion transporter family member 1c1, Mm00451845_m1), *Slc7a5* or *Lat1* (L-type amino acid transporter 1, Mm00441516_m1), *Slc7a8* or *Lat2* (L-type amino acid transporter 2, Mm01318974_m1), *Slc16a2* or *Mct8* (Monocarboxylate transporter 8, Mm00486204_m1) and *Slc16a10* or *Mct10* (Monocarboxylate transporter 10, Mm00661045_m1). Data were expressed relative to the mean values obtained in tissues from the WT mice (taken as 1.0) after correction for *18S* RNA.

2.5. Immunohistochemistry

The same protocol was followed for the following primary antibodies: Parvalbumin (1:1,500; P3088, Sigma-Aldrich), Calbindin (1:1,000; C9848, Sigma-Aldrich), Calretinin (1:4,000; 6B3, Swant), GAD65/67 (1:1,000; A01437, GenScript), and NeuN (1:2,000; MAB377, Chemicon). WT, P253L and *Mct8* KO mice tissues were processed in parallel. Endogenous peroxidase was blocked by incubating in dark with 3% hydrogen peroxide and 10% methanol in PBS at room temperature (RT) for 15 min. Nonspecific antibody binding was prevented by blocking with 4% BSA, 0.1% TritonX-100, 0.1 M Lysin and 5% serum from the secondary antibody host species at RT for 1 h. Sections were incubated overnight at 4 °C with primary antibodies in 4% BSA, 0.1% TritonX-100 and 1% serum. Tissues were incubated with biotinylated secondary antibodies at 1:200 concentration in 4% BSA, 0.1% TritonX-100 and 1% serum at RT for 1 h. For signal amplification, the sections were incubated with Avidin-Biotin Complex (ABC Elite Kit Vector Laboratories, #32050) in dark at RT for 1 h and developed with 0.5 mg/mL diaminobenzidine (Sigma, D5637) and 0.01% hydrogen peroxide. Finally, sections were dehydrated in ascending ethanol concentrations, cleared in xylenes, and covered with hydrophobic mounting medium Depex (Serva, 18243). Images for immunohistochemistry were obtained with a Nikon Eclipse 80i microscope and a Nikon DSFi1 digital camera.

All the preparations were then analyzed and quantified by means of Neurolucida® (MBF Bioscience, Vermont, USA) in a Nikon Eclipse E400 microscope with a Lumina HR camera (Lt665RC, MBF Bioscience, Vermont, USA) as described in Tapias et al. (2013), using a 20× objective (0.50 N.A.). For the quantification of immunopositive cells, every tenth section was sampled in each animal (an average of 5 histological sections per animal). The regions of interest (ROIs) were delineated based on a coronal atlas of the mouse brain (Paxinos and Franklin, 2004) and both hemispheres were analyzed. These ROIs spanned the entire cerebral cortex (layers 1 to 6) from Bregma −1 to Bregma −2.5 and the CA1 region of the hippocampus from Bregma −1.3 to Bregma −2.3.

NeuN expression was quantified similarly to what was described in Mayerl et al. (2014) as follows. Originating at the corpus callosum, a line was drawn at a right angle to the pial surface at four different places within the barrel field to quantify the thickness of the cortex. Moreover, additional shorter lines were drawn at the same positions starting from the corpus callosum to the border of layer IV to measure the dimension of the inner layers and the outer layers.

For GAD65/67 preparations, mean intensity was quantified as described in Valcárcel-Hernández et al. (2022).

2.6. Motor tasks assessment

For motor task analysis, WT ($n = 10$), P253L ($n = 8$) and *Mct8* KO ($n = 6$) mice at 3 and 6 months of age performed the tests described in this section.

2.6.1. Footprint test

The gait of the mice was evaluated using the footprint test as previously described (Bárez-López et al., 2014). The hind and the forepaws were painted with blue and red nontoxic waterproof paint, respectively, and the animals were required to run along a tunnel (20 × 20 × 70 cm) lined with paper, with a dark goal box at the end of the tunnel to encourage the mouse to run toward a dark and safe environment. Measurements for three-step cycles were averaged, considering a cycle as the distance from one pair of hind prints to the next. Footprints at the start and the end of the tunnel were excluded from the analysis as they correspond to the initiation and termination of the movement. The front base width, hind base width, forelimb stride length, hindlimb stride length and overlap of hind and forelimb were analyzed.

2.6.2. Four limb hanging wire test

Muscle strength was evaluated using the hanging wire test (Bárez-López et al., 2019; Crawley, 2006). Mice were placed on the top of a wire cage lid quadrant (14 × 14 cm) that was inverted horizontally 50 cm above a surface with bedding to avoid damage associated to the fall. The latency to fall was recorded over a maximum period of 120 s. Mice were tested for 2 consecutive days in 1 trial per day. Data from both days were averaged.

2.6.3. Rotarod test

Motor coordination and balance were evaluated with the accelerating-rotarod test as previously described (Bárez-López et al., 2014, 2019). Sixty min before the test, animals were subjected to an initial training period under constant speed. For the accelerated rotarod test, mice were placed on a rotarod (Ugo Basile, Italy) that accelerated from 4 to 44 rpm in 3 min and was maintained at 44 rpm for 2 further min. The latency of the mice to fall off the rod was recorded over the maximum observation period of 5 min. Mice were tested for 5 consecutive days with 3 trials per day with a 20 min intertrial interval. Data from the three trials were then averaged.

2.6.4. Balance beam test

Balance was evaluated as described (Arqué et al., 2009; Bárez-López et al., 2019). Mice were placed on the center of a horizontal wooden bar (0.9 cm wide × 50 cm long) 40 cm above a surface with bedding to avoid damage associated to the fall. The latency to fall was recorded over a maximum period of 40 s and 2 trials were performed in 1 single day. The activity on the bar was rated as [0] if the mouse fell, [1] if it remained in the center of the bar, [2] if it moved but it did not reach the ends; and [3] if the mouse reached one of the ends of the bar.

2.7. Behavioral tests

For behavioral tests, WT ($n = 10$), P253L ($n = 8$) and *Mct8* KO ($n = 6$) mice at 3 and 6 months of age performed the tests described in this section.

2.7.1. Elevated plus maze

Elevated-plus maze exploration was evaluated as described (Bárez-López et al., 2017a; Lister, 1987). In the present experiment, each mouse was placed in the center of a grey PVC elevated-plus maze (each arm 30 cm long and 5 cm wide, with 30-cm-high walls on closed arms, 50 cm high over the ground. The behavior of the mouse was videoed from above for 10 min. The mouse was then returned to its home cage. The videos were then analyzed by means of the software Ethovision® (Noldus, Wageningen, Netherlands) to study the time spent and the frequency to enter the open and closed arms of the maze.

2.7.2. Open field

Open field exploration was evaluated as described (Bárez-López et al., 2017a; Richard et al., 2017). In the present experiment, the open field apparatus was an empty 40 × 40 cm grey PVC arena with 30-cm-high walls. Each mouse was placed in the center of the apparatus and videoed from above for 10 min. The mouse was then returned to its home cage. All videos were obtained with a Microsoft LifeCam Studio camera (Microsoft Corporation, Redmond, WA, USA), and then analyzed by means of the software Ethovision® (Noldus, Wageningen, Netherlands) to quantify the distance walked by the animals, along with the time spent in both the central area of the field and the area closer to the walls.

2.8. Hearing and audiogenic seizure studies

2.8.1. Hearing assessment and noise exposure

Hearing was evaluated by recording the evoked auditory brainstem response (ABR) to sound with a System III Evoked Potential Workstation (Tucker-Davis Technologies, Alachua, FL, USA), as described (Cediel et al., 2006). Briefly, mice were anesthetized with ketamine (100 mg/kg) and xylazine (10 mg/kg) and placed on a heating pad inside a soundproof acoustic chamber. Click and 8-, 16-, 20-, 28-, and 40- kHz pure tone stimuli were presented at a decreasing intensity range from 90 to 20 dB sound pressure level. The electroencephalographic activity was recorded, amplified, and averaged to determine hearing thresholds, latencies, and amplitudes of the evoked waves.

2.8.2. Audiogenic seizure assays

As seizures are a common symptom exhibited by some MCT8-deficient patients, we assessed seizure susceptibility. To induce audiogenic kindling, mice were introduced in a soundproof acoustic chamber and allowed to explore for 30 s, and then exposed to repeated acoustic stimulation (2–20 kHz) of maximal intensity (120–130 dB). The sound was maintained until the running seizure was elicited. If no convulsions occur, the sound is applied for 90 s. Seizure behavior was defined as self-sustained explosive running which started with some delay after sound stimulation (seizure latency) and was followed or not by clonic seizure. The intensity of response was categorized as follows: no response (0); wild running (1); clonic seizure (2); tonic seizure (3); and respiratory arrest (4). Animals were tested only once at the end of the other evaluations.

2.9. Statistics

Data were expressed as mean ± SEM. Statistical analyses were performed with GraphPad Software (www.graphpad.com). Assessment of the normality of data was performed by the Shapiro-Wilk test. Means of *Mct8* expression levels were compared between WT and P253L groups by Student *t*-test. Means between all of the experimental groups were compared by the Kruskal-Wallis test for non-parametric data, or one-way ANOVA for parametric data. For motor and behavior tests, repeated measures from all the experimental groups at P90 and P180 were analyzed by two-way ANOVA. Significant differences were represented as $^{*}P < 0.05$; $^{**}P < 0.01$, and $^{***}P < 0.001$ or indicating the exact p value for values close to 0.05.

2.10. Study approval

Animal studies: all experimental procedures involving animals were performed following the European Union Council guidelines (directive 2010/63/UE) and Spanish regulations (R.D. 53/2013), and were

approved by the ethics committee Comité de Ética y Experimentación Humana y Animal (CEEHA) at Consejo Superior de Investigaciones Científicas (CSIC) and by the Comunidad Autónoma de Madrid Review Board (Proex 014.1/21) for the use of animals for scientific purposes.

3. Results

3.1. P321L is a conserved residue and its mutation results in structural alterations in the MCT8 protein

To elucidate the biological importance of the P321 residue, we explored its evolutionary conservation by performing an alignment with several MCT8 orthologues and the other human MCT family transporters. This alignment showed that this residue is highly conserved, being present in all the available MCT8 orthologues and other MCTs such as MCT10 and MCT5 (Supplemental Fig. 1).

Given the high evolutionary conservation of the P321 residue, we assessed its structural and functional importance *in silico*. For this, human and mouse MCT8 proteins were modeled by comparison with the outward-open conformation of MCT1 (RCSB's Protein Data Bank code 6LYY, (Wang et al., 2021)) (Fig. 1A) and MCT2 (PDB code 7BP3, (Zhang et al., 2020) data not shown) structures obtained by cryo-electron microscopy. MCT8 models were obtained with the recent CASP14 best performing server Robetta, created by the Baker Lab (Baek et al., 2021). The MCT1 model was finally selected as a template over MCT2 due to its superior structural homology. Both human and mouse MCT8 are β-barrel proteins, with 12 TMHs disposed in two 6-helices symmetric bundles with an inner pocket placed between them. Because there were hardly any differences in the MCT8 protein between both species, we decided to continue the analysis only with the human one.

Intriguingly, the P321L mutation impairs T3 uptake (Kersseboom et al., 2013; Vatine et al., 2019, 2017) even though this residue is not close to the described binding region for T3 or T4 in the MCT8 protein. This suggests that P321L mutation affects the protein structure itself, rather than the THs binding region directly. To test this, we performed prediction *in silico* analyses of the structure of the MCT8-P321L mutation, where Robetta prediction for MCT8-P321L showed a structure almost identical to the wild-type. Both homology models, MCT8 and MCT8-P321L were validated by means of VERIFY3D, PROCHECK and ERRAT2 servers (for further information see Methods section and Supplemental Fig. 2A, B, C, D). However, 3D-alignment between MCT8 and MCT8-P321L models revealed a decrease in the distance between TMHs in the mutant (Fig. 1B). Distance between TMHs is a crucial parameter for protein structure, especially for proteins with a rocker switch mechanism, such as MCT8 (Schweizer et al., 2014), which experience a sequence of conformational changes to allow T3 and T4 to access the central binding site from both sides of the cell membrane. To gain further insights into the structural change, intra-protein interactions of both MCT8 and MCT8-P321L models were then assessed by means of RINGS 2.0 (Martin et al., 2011; Piovesan et al., 2016), which predicted five new interactions between amino acids when the P321L mutation was introduced (Fig. 1B, Supplemental Fig. 2E) as compared to wild-type MCT8. According to this prediction, the mutated leucine 321 can interact with the residues I197 from TMH1 and W431, L434 and V435 from TMH8. Notably, some of these interactions comprise hydrogen bonds, which can explain the structural change, since they are strong enough to provoke a reduction in the distance of the interacting TMHs. Particularly interesting is the hydrogen bond generated between L321 and W431 since, in cooperation with L434 and V435 interactions, provokes the approach of TMH2 and TMH8 and closes up both bundles of MCT8 leading to morphological alterations in the pocket placed between them (Supplemental Fig. 2E). Further analysis showed a dramatic reduction in the pocket size with an aberrant form in which the entrance of the pocket is not connected to the central substrate-binding region (Fig. 1C). According to this prediction, in MCT8-P321L, THs would no longer be able to access the binding site of MCT8. In addition to affecting the size and shape of the pocket, the appearance of new binds between the two bundles of MCT8 may cause an increase in the rigidity of the structure preventing the conformational changes necessary to perform its function in the transport of T3 and T4.

3.2. P253L mice present abnormal T3 and T4 levels/content in plasma and tissues

Postnatal day 90 (P90) P253L mice presented peripheral TH alterations similar to the ones observed in *Mct8* KO mice, showing high T3 (78% higher) and low T4 (45% lower) plasma levels, as well as high T3 (68% higher) and low T4 (28% lower) content in liver, in comparison with WT mice (Fig. 2). All these data resemble the peripheral thyroid state of MCT8-deficient patients.

Moreover, the study of T3 and T4 content in the CNS revealed that P253L mice present a significant reduction in the T3 content in the cerebral cortex (31% lower) in comparison to WT animals, similar to *Mct8* KO mice as previously found (Dumitrescu et al., 2006; Trajkovic et al., 2007). Surprisingly, P253L mice also presented a significant reduction in T4 content (40% lower) as compared to WT animals, in contrast to *Mct8* KO mice, which did not present alterations in the content of T4. Given the complexity of the CNS, and the locomotor impairments exhibited by the patients we decided to also study the cerebellum. The analysis of TH content revealed that P253L mice present a significant reduction in the T3 content (50% lower) in comparison to their WT counterparts, similarly to *Mct8* KO mice as previously observed (Trajkovic et al., 2007). However, there were no differences in the content of T4 between none of the studied genotypes.

3.3. P253L mice do not show alterations in TH-target genes

Following the thyroid status evaluation, we decided to assess the expression of several genes which have already been confirmed to be dependent on the thyroid status (TH-target genes) in the brain (Morte et al., 2010b; Zada et al., 2014). To this aim, we analyzed by quantitative PCR all the three experimental groups: WT, P253L and *Mct8* KO mice at P90, particularly for the expression of 8 genes in the cerebral cortex: *Cbr2, Cntn2, Hr, Dio3, Nefm, Dio2, Flywch2,* and *Mbp*. These results revealed that P253L mice do not present significant alterations in gene expression, in contrast to *Mct8* KO mice, as compared to WT mice (Fig. 3). Of the 8 genes, *Cbr2, Cntn2* and *Hr* were sensitive to MCT8 deficiency at P90 in the *Mct8* KO mice, consistent with previous findings (Morte et al., 2010b). *Dio3* showed subtle reduced expression in *Mct8* KO mice compared to WT levels which was not statistically significant. The rest of the analyzed genes (*Nefm, Dio2, Flywch2,* and *Mbp*) did not reveal any differences between any of the experimental groups. This data indicated that the expression of the analyzed TH-target genes in the cerebral cortex of P253L mice is normal despite the alterations in TH content in this structure.

3.4. P253L mice show alterations in THs transporter's gene expression

Following the thyroid target genes evaluation, we assessed the expression of the genes encoding several TH transporters at P90. First, we analyzed by quantitative PCR *Mct8* expression on WT and P253L groups finding that in P253L mice, *Mct8* expression is decreased by half compared to WT mice (Fig. 4A). Then, we analyzed in WT, P253L, and *Mct8* KO mice the expression of other four genes encoding the TH transporters *Oatp1c1, Mct10, Lat1,* and *Lat2* in the cerebral cortex. We found that the expression of these genes in P253L mice was not different from WT values, whereas *Mct8* KO mice showed a significant increase in *Oatp1c1*and *Lat2* expression as compared to WT mice, and in *Oatp1c1* and *Lat1* expression in comparison to P253L mice (Fig. 4B).

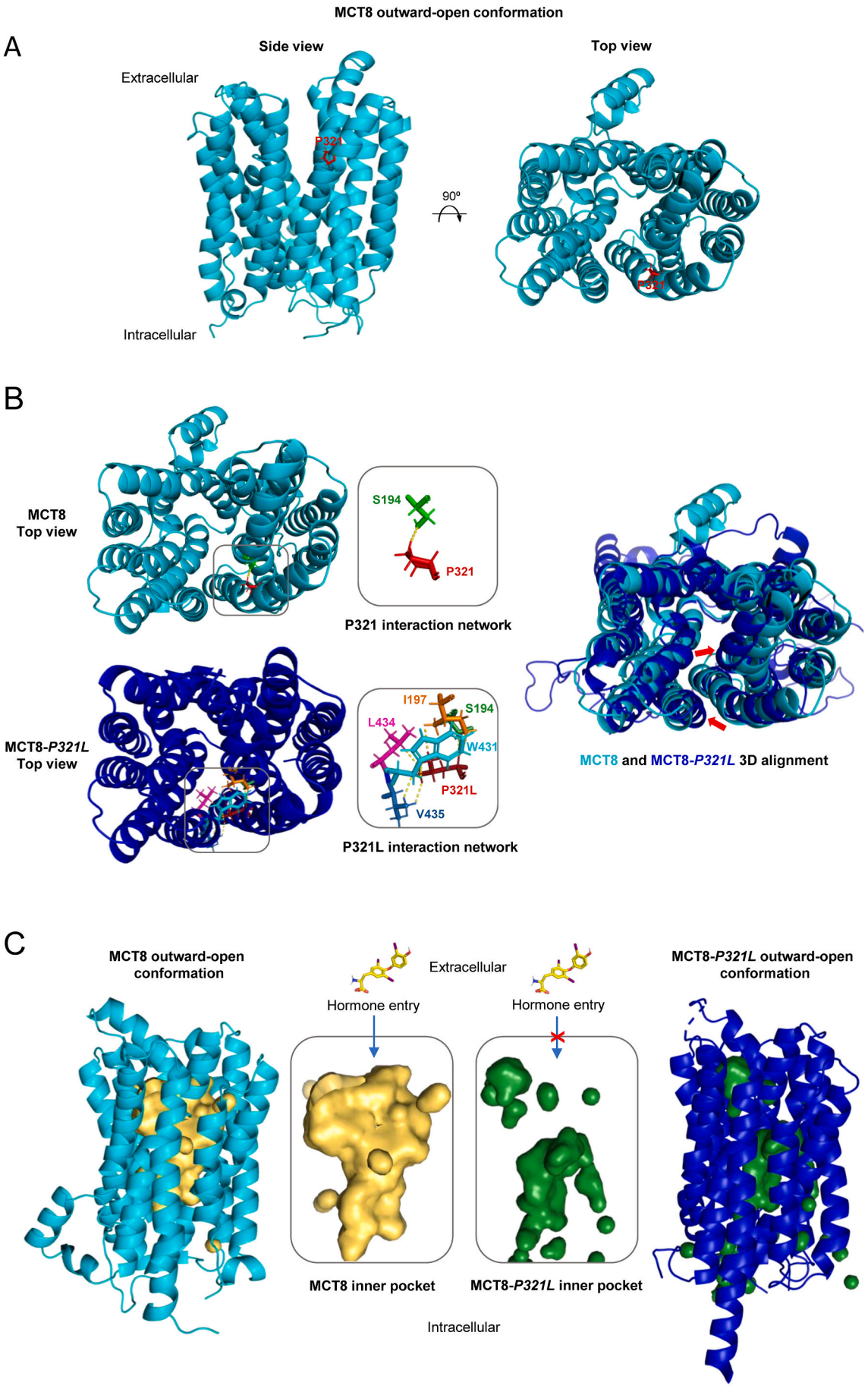

(caption on next page)

Fig. 1. Tertiary structure of MCT8 homology model in the outward-open conformation. (A) MCT8 structure was predicted using the Robetta server based on the cryo-electron microscopy structure of the outward-open conformation of human MCT1 (PDB: 6LYY). The model was refined to eliminate non-precisely predicted residues (>5 Å of error). Side (left) and top (right) cartoon views of the MCT8 structure were generated with PyMOL software. Proline 321, the residue mutated in two AHDS patients, is shown as red sticks. (B) 3D alignment of MCT8 (light blue) and MCT8-P321L (dark blue) models show a decrease in the distance between TMHs in the mutant. P321L mutation changes the amino acidic interaction network in MCT8. Changes in TMHs position between both models are indicated with red arrows (right panel). MCT8-P321L structure was predicted as described in A. 3D alignment was performed by means of Pymol software. P321L mutation changes the amino acidic interaction network in MCT8 (left panel). While P321 residue only interacts with S194 from TMH1, the P321L mutant also interacts with I197 from TMH1 and W431, L434, and V435 from TMH8. Intra-protein interactions of MCT8 and MCT8-P321L were assessed by RINGS 2.0 and the predicted amino acidic interaction networks were represented by Pymol. Residues are shown as colored sticks. (C) A comparison of the structure of the inner pocket of MCT8 (yellow) and MCT8-P321L (green) shows a dramatic change in the shape and size of the pocket. MCT8 (light blue) and MCT8-P321L (dark blue) are shown as cartoons with the inner cavity represented as a surface in yellow and green respectively. Hormone influx sense was represented by blue arrows. Triiodothyronine (T3) structure was represented as yellow sticks. CASTp server and PyMOL were used for substrate-binding pocket volume analysis and image generation. (For interpretation of the references to colour in this figure legend, the reader is referred to the web version of this article.)

3.5. P253L mice show altered neuroarchitecture

To assess the gross neuroarchitecture of P253L mice, samples from WT, P253L and *Mct8* KO mice brains at both P90 and P180 were immunolabeled with NeuN (Fig. 5). P180 age was selected as an adequate marker of full adult age, providing a reliable picture of persistent alterations after P90. No substantial changes were observed in the density of neurons in P253L mice as compared to WT animals. However, the distribution of neuronal layers was clearly altered, as P253L immunolabeling revealed less definition in the boundaries between layers, particularly between layers III and IV. Fine layer delimitation in these animals was difficult to establish. Consequently, to evaluate possible alterations in cortical cytoarchitecture we decided to quantify the thickness of layers I-IV on the somatosensory cortex, which could be accurately delimitated. Layers I–IV were significantly thinner in P253L animals at all time points (16% thinner at P90 and 13% thinner at P180), as compared to WT mice. However, no difference was found between P253L and *Mct8* KO animals or between WT and *Mct8* KO animals, suggesting that *Mct8* KO animals exhibit an intermediate phenotype.

3.6. P253L mice show impairments in the GABAergic system

The GABAergic system is a classical TH target (Gilbert and Lasley, 2013; Venero et al., 2005; Wallis et al., 2008), as well as a hallmark of MCT8 deficiency (López-Espíndola et al., 2014) and has been also reported to be affected in double mutant MCT8 deficiency animal models (Bárez-López et al., 2019; Mayerl et al., 2014). So, to assess the effect of the P253L mutation on GABAergic neurons, coronal sections of WT, P253L and *Mct8* KO mice brains at both P90 and P180 were immunostained against parvalbumin, calretinin, calbindin and glutamic acid decarboxylase (GAD) 65/67. Differences between experimental groups were studied in particular detail in the cerebral cortex. P253L mice showed important and statistically significant differences not only with the WT but also as compared to *Mct8* KO mice.

P253L mice present a significant decrease in the number of parvalbumin immunopositive neurons, as compared to WT (22% lower) at P90 (Fig. 5), and as compared to both WT and *Mct8* KO animals at P180 (9.2% and 23% lower respectively, see also Supplemental Fig. 3). This decrease appears to be widespread in the brain and not restricted to the cerebral cortex, as observed in other regions such as the hippocampus. In the hippocampal formation, particularly in the CA1 region, a significant decrease in parvalbumin positive cell density was observed in P253L mice and, surprisingly, also in the *Mct8* KO as compared to WT mice at P90 (Supplemental Fig. 4).

In the cerebral cortex P253L mice showed a significant decrease in the number of calbindin positive cells as compared to both WT and *Mct8* KO mice. The distribution pattern was also different, as P253L staining reveals fewer positive cells in inner layers (Layers V-VI) of the cortex, as well as a more diffuse, less grouped distribution in outer layers (Layers II-III) (Fig. 5). At P90, P253L mice present a 43% decrease in the number of calbindin positive neurons as compared to WT mice, as well as a 42% decrease as compared to *Mct8* KO animals. At P180, the calbindin positive neurons population was decreased by 19% as compared to WT mice. Moreover, the morphology of cortical calbindin-expressing cells appeared to be altered in P253L mice, as an important increase of ramifications and branching was observed, as compared to any of the other two studied genotypes (Fig. 5). In the hippocampal region, we focused on the CA3 region where we observed a decrease in calbindin immunopositive cell density in P253L mice as compared to WT and *Mct8* KO mice (Supplemental Fig. 5).

P253L mice showed a significant increase in the number of calretinin positive neurons in the cerebral cortex as compared to WT animals (Fig. 5). At P90, P253L mice present a 50% increase in the population of calretinin positive neurons as compared to WT mice. At P180, calretinin positive neuron number was increased by 40% as compared to WT mice. This increase also appears to be widespread throughout the brain, as observed particularly in the dentate gyrus (Supplemental Fig. 6).

In the motor cortex, P253L mice also showed a decrease in GAD65/67 staining intensity as compared to WT mice (Fig. 5). At P90, P253L mice present a 13% decrease in the expression of GAD65/67 as compared to WT mice and at P180 the expression of GAD65/67 was decreased by 18% as compared to WT mice. In the hippocampal formation, we focused on the dentate gyrus and CA3 region. In both areas, a decrease of GAD65/67 staining intensity was observed in P253L mice as compared to WT and *Mct8* KO mice (Supplemental Fig. 7).

3.7. P253L mice show altered behavior

To assess the possible effects of P253L mutation in the psychomotor phenotype we performed a battery of behavioral tests including footprint analysis, four limb hanging wire test, rotarod, balance beam, open-field and elevated plus maze tests on all three experimental groups.

The gait of the mice was evaluated using the footprint test at both P90 and P180. The front base width, hind base width, forelimb stride length, hind limb stride length and overlap of hind and forelimb were analyzed and none of them showed any difference between the experimental groups (Fig. 6A).

To evaluate muscle strength, the four-limb hanging wire test was performed revealing impairments in P253L mice as compared to WT mice. A significant decrease in the latency to fall from the grid was observed in P253L mice at P180, as this latency was 17% lower than the observed in WT mice. WT and *Mct8* KO mice did not present any differences between them in this parameter. No significant differences could be observed between groups at P90 (Fig. 6B).

Motor coordination and balance were evaluated using the rotarod test, also showing impairments in P253L mice as compared to both WT and *Mct8* KO mice. P253L mice showed a significant decrease in the latency to fall from the rotarod as compared to the other groups at P180, being this difference sustained in all 5 days of the experiment. The average time to fall was 23% lower than the one showed by WT mice and 26% lower than that of *Mct8* KO mice. However, at P90 no significant differences were observed between groups, even though a trend to fall off the rod before WT and *Mct8* KO mice was observed in the P253L mice

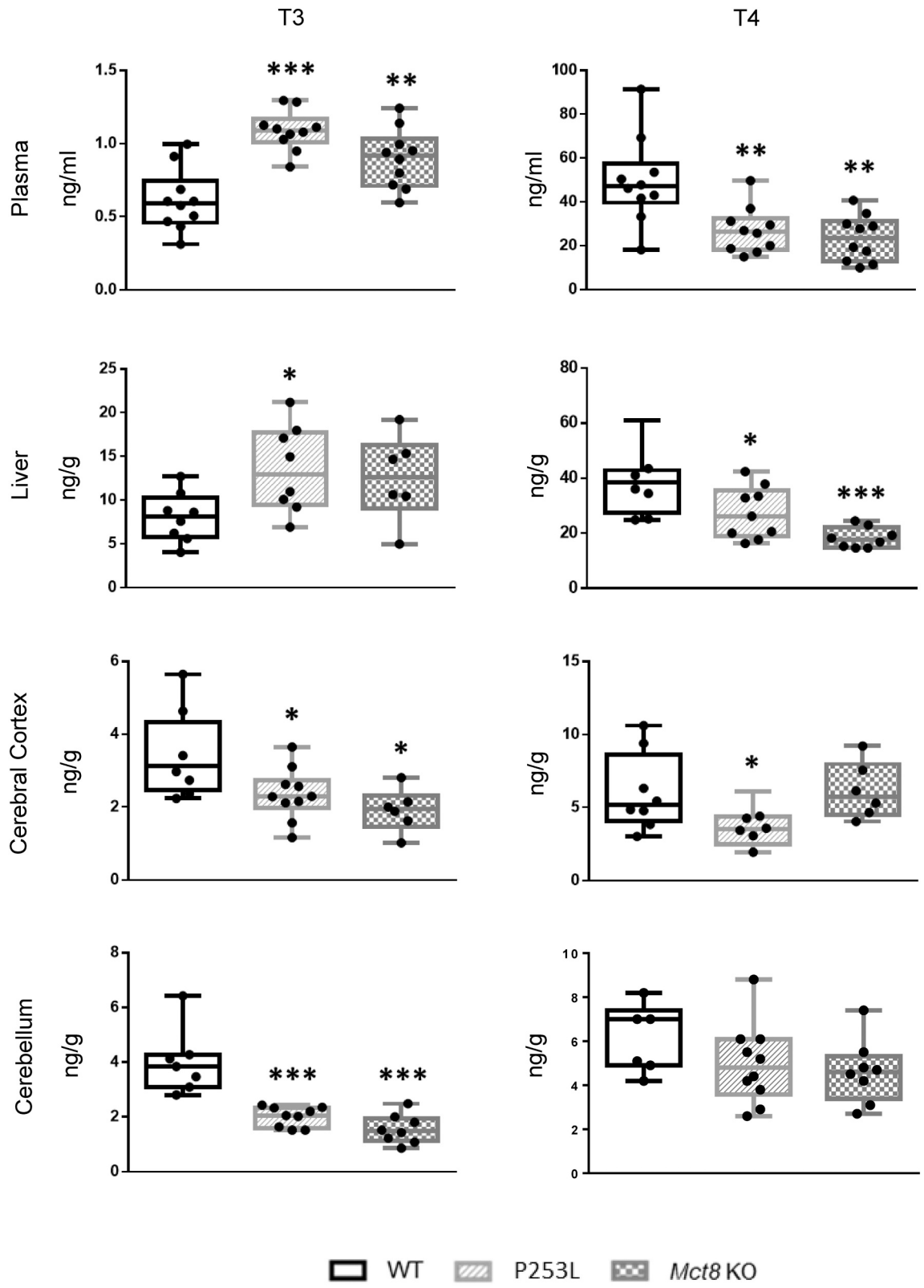

Fig. 2. Thyroxine (T4) and triiodothyronine (T3) levels/content in P90 WT, P253L and *Mct8* KO mice ($n = 10$, some samples were removed due to intra-sample variability) in plasma, liver, cerebral cortex and cerebellum. Measures were obtained by specific radioimmunoassays. *$P < 0.05$, **$P < 0.01$, and ***$P < 0.001$ indicate differences *versus* WT group and were determined by one-way ANOVA and Bonferroni's *post hoc* test.

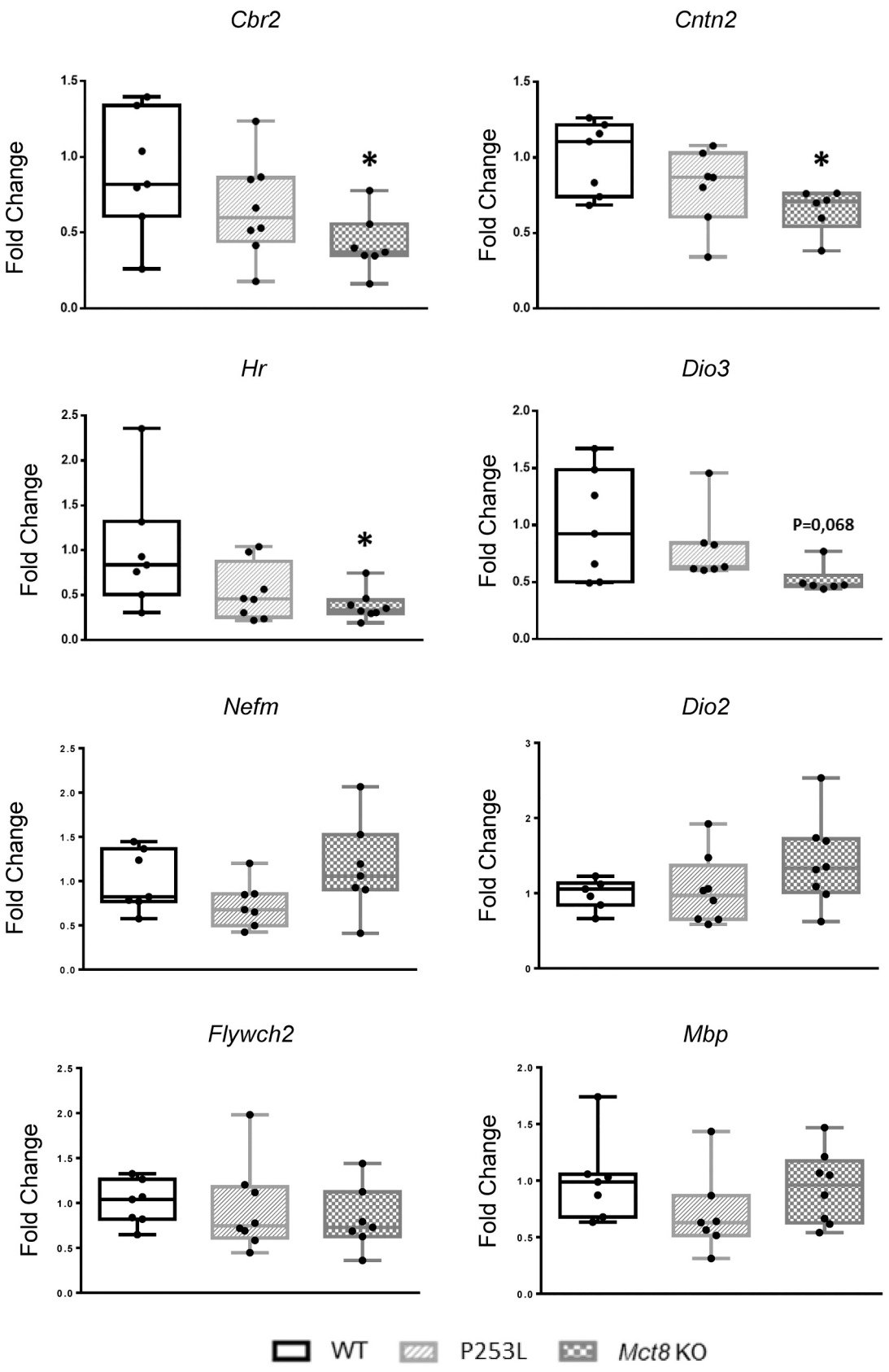

Fig. 3. Gene expression analysis of T3-dependent genes in the cerebral cortex in P90 WT, P253L and *Mct8* KO mice ($n = 8$). Measurements were obtained by quantitative PCR, and the data are expressed relative to *18S* RNA and as Fold Change *versus* mean WT values. *$P < 0.05$ indicates differences *versus* WT group and were determined by one-way ANOVA and Bonferroni's *post hoc* test.

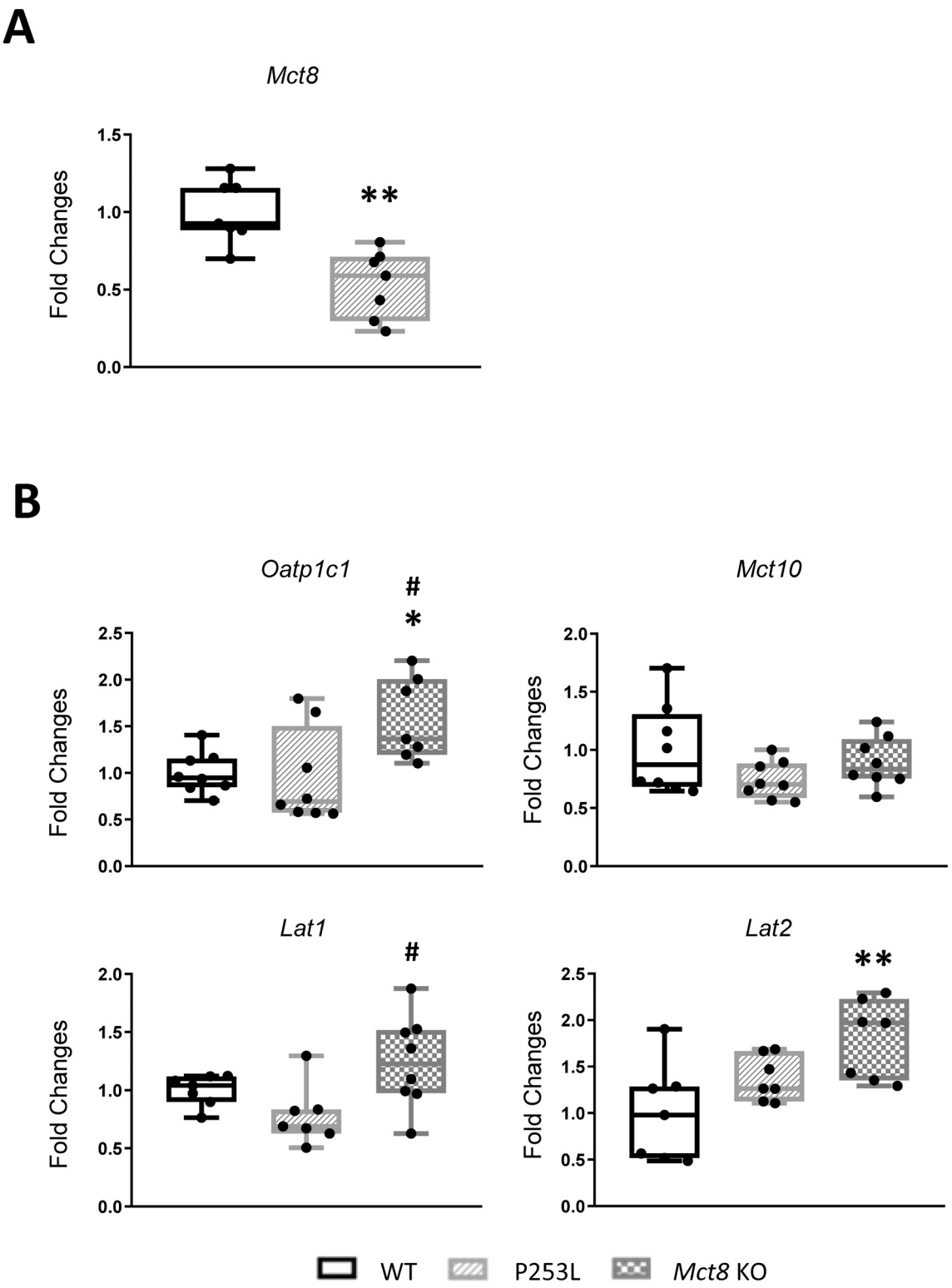

Fig. 4. A. *Mct8* expression analysis in P90 WT and P253L mice (n = 8). B. Gene expression analysis of other TH transporter genes in the cerebral cortex in P90 WT, P253L and *Mct8* KO mice (n = 8). The following samples were removed from the analysis after outlier identifying with ROUT: one animal per group for *Mct8* and *Lat2*, one *Mct8* KO animal in *Oatp1c1* and one P253L in *Lat1*. Measurements were obtained by quantitative PCR, and the data are expressed relative to *18S* RNA and as Fold Change *versus* mean WT values. $^{*}P < 0.05$ and $^{**}P < 0.01$ indicate differences *versus* the WT group and #P < 0.05 *versus* the P253L group that were determined by one-way ANOVA and Bonferroni's *post hoc* test, except for *Mct8* expression levels by Student *t*-test.

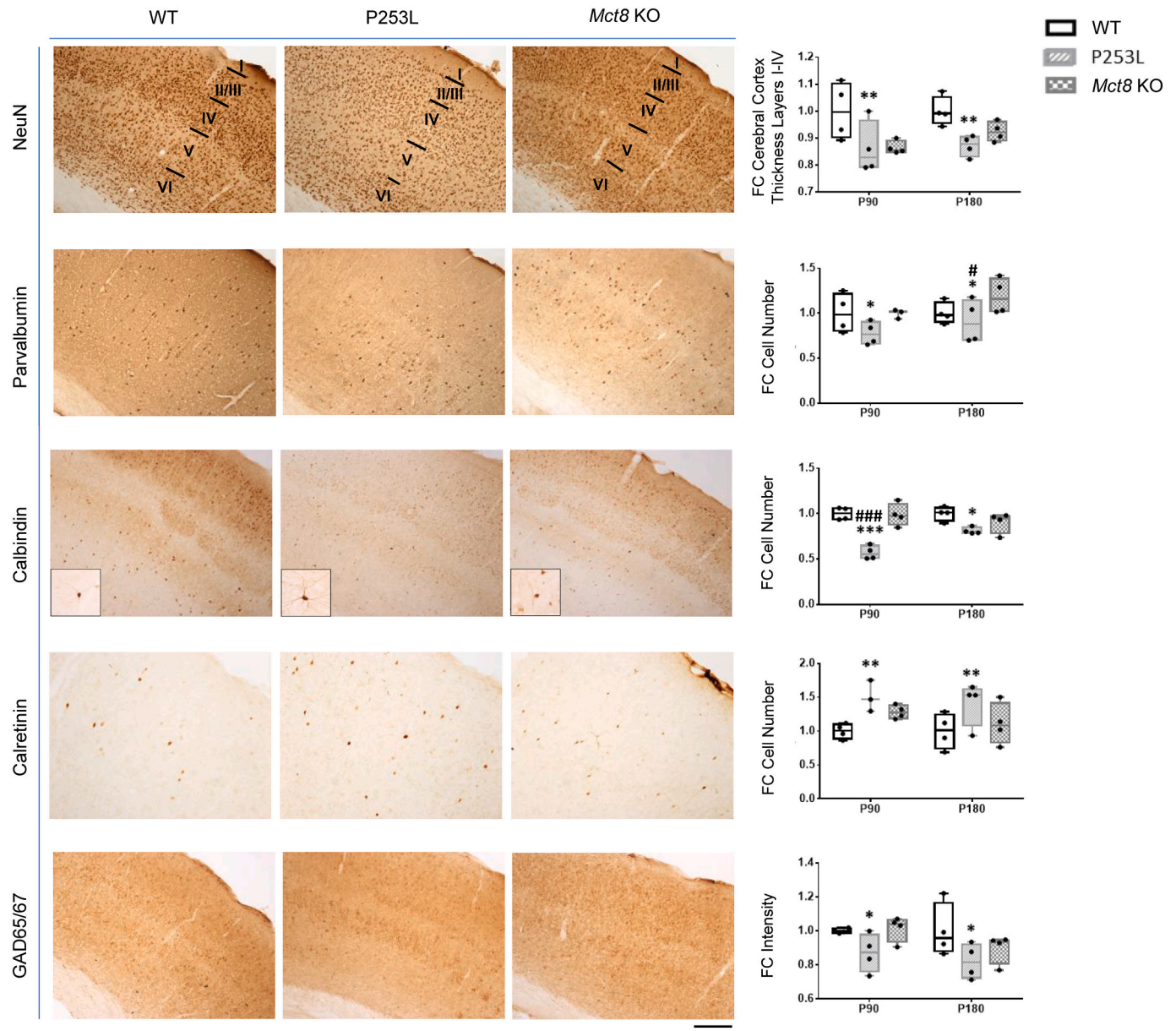

Fig. 5. Histological analysis of GABAergic neurons in the somatosensory cortex. Coronal brain sections from P90 and P180 WT, P253L and *Mct8* KO mice ($n = 4$) were immunostained with antibodies recognizing the neuronal transcription factor NeuN, the calcium-binding proteins parvalbumin, calbindin, and calretinin and the GABA-producing enzyme GAD65/67. Representative images depict the expression of NeuN, parvalbumin, calbindin, calretinin and GAD65/67 in the somatosensory cortex at P90 (see Supplemental Fig. 3 for P180 images). Cerebral cortex layers are defined in the first row. Insets depict individual calbindin positive cells. Scale bar represents 500 μm except in calbindin insets and calretinin images, 250 μm. Graphs on the right represent the thickness of the cortical layers determined in NeuN-stained brain sections, the number of parvalbumin, calbindin and calretinin immunopositive cells and GAD65/67 signal intensity as fold change compared to the WT group, at both P90 and P180. $*P < 0.05$, $**P < 0.01$, $***P < 0.001$ indicate differences *versus* WT group, #P < 0.05 ###P < 0.001 indicate differences *versus Mct8 KO* group and were obtained by one-way ANOVA and Bonferroni's *post hoc* test, except for parvalbumin and calretinin which were obtained by Kruskal-Wallis test. FC: Fold change.

(Fig. 6C).

Balance beam test was performed also at both P90 and P180. This test showed no difference in the latency to fall from the beam between genotypes, as no mice fell during the experiment at either P90 or P180 (data not shown).

The exploratory and anxiety-like behavior was assessed using the elevated plus maze on all the experimental groups as a decrease in the willingness to explore the open arms of the maze is a classical parameter to determine anxiety. P253L mice exhibited an abnormal behavior when subjected to this test, as compared to WT mice. P253L mice showed at P180 an increase in the time spent in the closed arms of the maze, along with a decrease in the frequency to exit those arms and enter the open arms, as compared to WT mice (Fig. 7A, B). This difference reveals an anxiety-like behavior in P253L mice. At P90 all these differences, however, were not observed between any of the studied groups.

To further test the exploratory behavior, the open-field test was performed on all the experimental groups. No difference between groups was observed neither at P90 nor at P180 (Fig. 7C).

3.8. P253L mice have no auditory defects

To assess the possible effects of P253L mutation in audition, as other MCT8-deficiency animal models have shown alterations in this parameter (Sharlin et al., 2018) all the experimental groups were subjected to

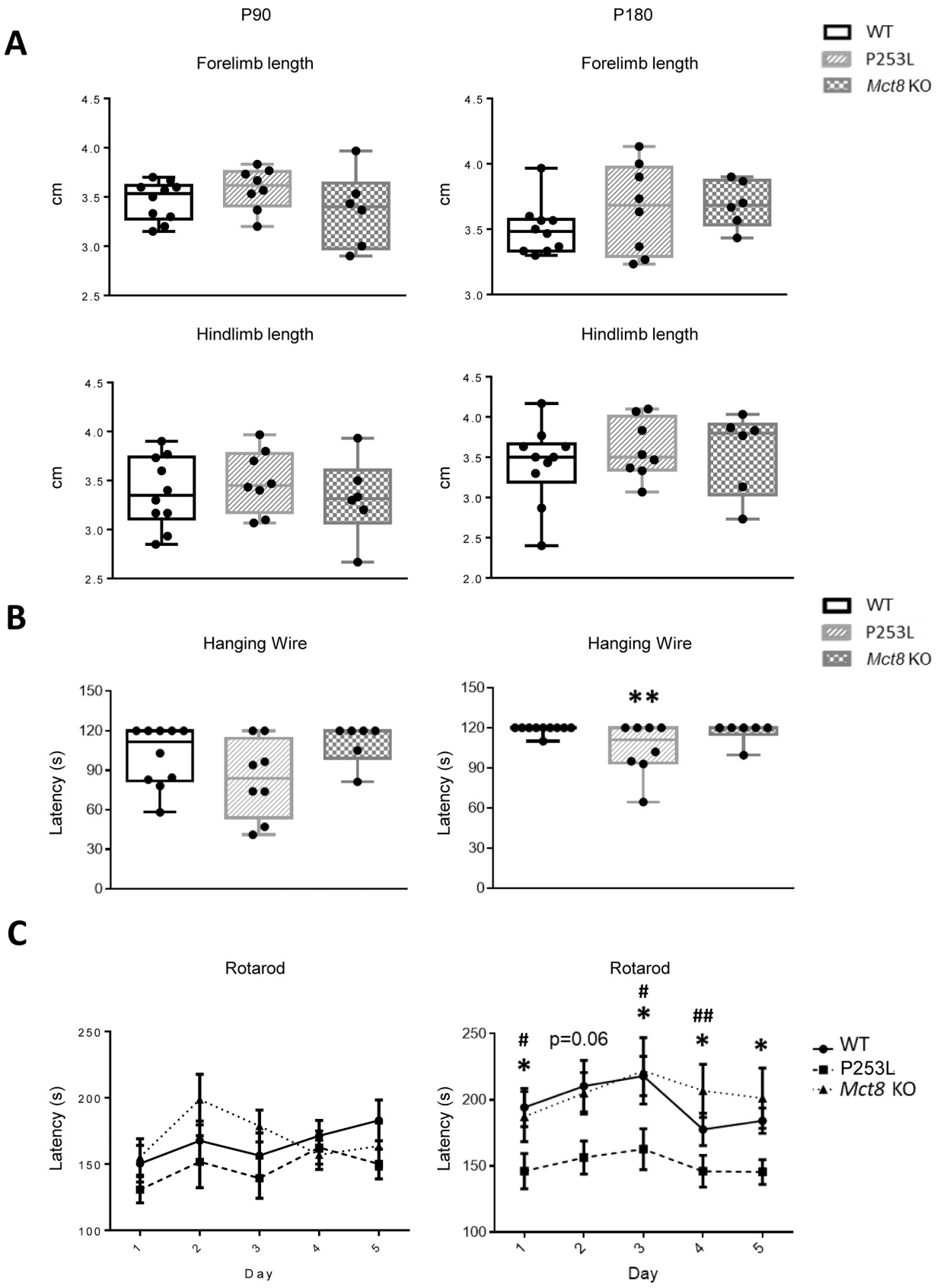

Fig. 6. Evaluation of coordination, muscle strength and motor performance. WT (n = 10), P253L (n = 8) and *Mct8* KO (*n* = 6) mice were subjected to footprint, hanging wire and rotarod tests at both P90 and P180. Graphs depict forelimb step length and hindlimb step length in the footprint test (A), latency to fall from the grid in the hanging wire test (B) and latency to fall from the rotarod (C). *$P < 0.05$, **$P < 0.01$ indicate differences *versus* the WT group, #P < 0.05 ##P < 0.01 indicate differences *versus* the *Mct8 KO* group and were obtained by one-way ANOVA (hanging wire test) or two-way ANOVA (rotarod) and Bonferroni's *post hoc* test.

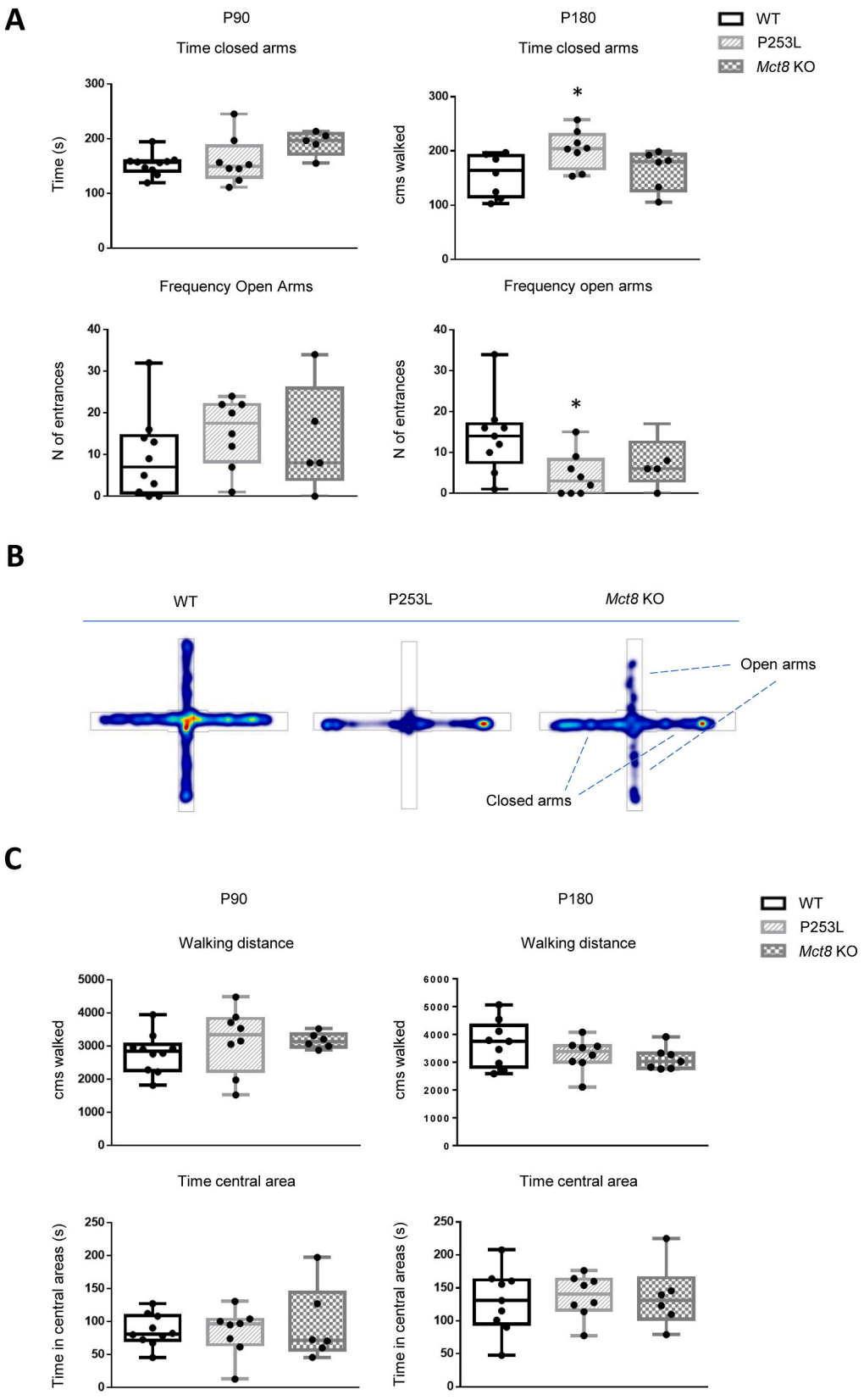

Fig. 7. Evaluation of anxiety-like phenotype. WT (n = 10), P253L (n = 8) and *Mct8* KO (n = 6) mice were subjected to open field and elevated plus maze tests at both P90 and P180. (A) Graphs depict time in closed arms and frequency to exit into the open arms of the elevated plus maze. (B) Images depict average heatmaps for all of the experimental groups in elevated plus maze assay at P180. (C) Graphs depict walked distance and time in the central area of the open field *$P < 0.05$ indicates differences *versus* the WT group and was obtained by two-way ANOVA and Bonferroni's *post hoc* test.

ABR test, an evoked-potentials based test that allows fast, reproducible, quantitative and non-invasive assessment of auditory function both on the reception of the stimuli and the transmission to auditory nuclei in the brainstem (Cediel et al., 2006).

Auditory function was evaluated at P90 using two kinds of stimulation. Click stimulation, where the auditory stimulus is unspecific and composed by the whole audible frequencies' spectrum, and pure tone stimulus, where a specific frequency stimulates a specific Corti organ region.

The auditory evaluation did not reveal any alterations in the auditory thresholds, neither in click assays (Supplemental Fig. 8A) nor in the pure tone audiogram (Supplemental Fig. 8B), suggesting a normal auditory function in P253L and *Mct8* KO mice.

3.9. P253L mice are not prone to audiogenic epilepsy

As seizures are one common symptom among some of the MCT8-deficient patients (Masnada et al., 2022) we decided to subject P253L and *Mct8* KO mice to a well-established assay to evaluate epilepsy propension. To induce audiogenic kindling, P90 WT, P253L and *Mct8* KO mice were exposed to high-intensity acoustic stimulation. Neither genotype showed any propensity to audiogenic-induced seizures, as they endured the whole 90 s of stimulus without showing any kindling (data not shown).

4. Discussion

In response to the need to obtain optimal mammalian models to explore the pathophysiology and therapeutic approaches for the AHDS, we have characterized a new murine model generated by introducing with CRISPR/Cas9 a point mutation present in two AHDS patients with a severe neurological phenotype.

Our alignment analysis of the residue altered in the chosen mutation (P321L) indicates that it is a well conserved amino acid among the different MCT8 orthologues (Groeneweg et al., 2019a; Vaurs-Barrière et al., 2009) and also in other transporters of the MCT family (Kinne et al., 2010; Kleinau et al., 2011), indicating the importance of this particular amino acid. Previous studies demonstrated that even though the P321L-mutated MCT8 protein can reach the plasma membrane and that the mutation is not located in a residue crucial to the on/off switch in the conformation (Kinne et al., 2010), the resulting protein has impaired T3 transport capability and disturbed mobility across the membrane (Kersseboom et al., 2013). We now demonstrate by protein structure prediction analysis that P321L mutation (P253 in mice) alters MCT8 structure by establishing bonds between the leucine and conserved residues from other TMHs that are not present in the original protein. Alterations produced by substituting a proline with a leucine have already been reported to lead to significant structural and functional alterations in other proteins (Yin et al., 2021), which were already suggested for MCT8 (Kleinau et al., 2011). These interactions would also provoke several conserved sequences to change their original orientations within the molecule, altering the whole protein structure, which eventually could lead to the loss of function in the protein described *in vitro* (Kersseboom et al., 2013). In our prediction, the generation of these new bonds would lead to a reduction in the distance between both bundles that conform MCT8 structure, severely affecting the size and shape of the substrate binding pocket. These new bonds could also reduce the flexibility of the MCT8 structure and alter the switch between inward/onward conformations. All these features are potential mechanisms underlying the loss of function of P321L-mutated-MCT8.

We have found that P253L mice mimic the thyroid profile characteristic of MCT8-deficient patients with peripheral hyperthyroidism along with decreased brain T3 content. The decrease in T3 brain content is in agreement with previous *in vitro* studies showing T3 transport impairments in the presence of MCT8 P321L mutation (Kersseboom et al., 2013) and supports our *in silico* prediction model. Moreover, a decrease in the content of T4 was also observed in the cerebral cortex, mimicking the decrease observed in AHDS patients (López-Espíndola et al., 2014) possibly due to the absence of an increase in the expression of *Oatp1c1* and *Lat2* transporter genes, which do increase in *Mct8* KO mice.

In both *Mct8* KO and P253L mice additional transporters at the brain BBB can compensate to some extent for the lack of MCT8 function. The study of genes encoding TH transporters revealed that the expression of *Mct8* in P253L mice was decreased, consistent with observations in iPSC-derived brain microvascular endothelial-like cells carrying this mutation by Braun et al. (2022). Interestingly the expression of *Oatp1c1* and *Lat2* transporter genes did not increase in P253L mice in contrast to *Mct8* KO animals, which may be hindering the ability of the TH transport system to compensate for the absence of MCT8-dependent transport. Indeed, histological analyses performed for different neuronal markers indicated that the general neuroarchitecture and the GABAergic system were impaired in P253L animals, but not in *Mct8* KO mice. P253L mice presented impairments in the definition and thickness of the layers of the cerebral cortex. The GABAergic system, a classical TH target (Gilbert et al., 2007; Venero et al., 2005; Wallis et al., 2008), showed alterations observed in other brain hypothyroid models, such as *Mct8/Dio2* KO and *Mct8/Oatp1c1* KO mice (Bárez-López et al., 2019; Mayerl et al., 2014) and other thyroid-related models (Hadjab-Lallemend et al., 2010; Venero et al., 2005; Wallis et al., 2008) and were consistent with the ones observed in AHDS patients (López-Espíndola et al., 2014). Such severe alterations in the GABAergic system could be altering the balance between inhibition and excitation in the CNS, impairing crucial events in cortical function and plasticity, as seen in other neurological and neuropsychiatric diseases such as depression, schizophrenia and autism (Lehmann et al., 2012). Seizures have been commonly reported as a symptom of the AHDS (Groeneweg et al., 2020; Masnada et al., 2022; Remerand et al., 2019) and GABAergic alterations, including those present in other animal models with impaired TH-action, have already been related to epilepsy (DeFelipe, 1999; Kaila et al., 2014; Tamijani et al., 2015). Even though patients with P321L mutations have not been reported to be epilepsy-prone (Vaurs-Barrière et al., 2009; Verge et al., 2012) consistent with our current findings in the P253L mice, alterations in the GABAergic system could be underlying the predisposition to epilepsy in some patients.

Similar to the findings at the histological level, P253L mice presented important impairments in motor and emotional behavior that were not observed in *Mct8* KO mice. We found a late-onset motor and emotional phenotype in P253L mice that presented impairments in muscle strength, limb coordination and anxiety. Alterations in motor function in P253L mice are consistent with the observations in AHDS patients as movement disorders are one of the hallmarks of the disease (Grijota-Martínez et al., 2020; Masnada et al., 2022), further confirming the suitability of these mice as a model of AHDS. The presence of anxiety-like behavior in *Mct8* KO mice is a controversial point, as it has been reported both a decrease in anxiety in male KO mice (Wirth et al., 2009) and an increase in anxiety in female KO mice (Mayerl et al., 2022). No emotional alterations were observed in *Mct8* KO mice, in contrast to P253L mice that presented an increased anxiety-like behavior based on the decreased willingness to exit the open arms in the elevated plus maze but no impairments in their exploratory behavior as seen in the open-field test. A potential mechanism leading to anxiety disorders in P253L mice could be the impaired parvalbumin expression in the CA1 area, as observed in a TRα1 mutant model (Venero et al., 2005). Another classical feature associated to alterations in THs availability and action is auditory impairments (Hébert et al., 1985; Ng et al., 2004; Sharlin et al., 2018), although in MCT8 deficiency this feature has only been reported once (Gagliardi et al., 2015). In contrast to the results obtained in *Mct8* KO mice (Sharlin et al., 2018) and other models with impairment of thyroid signaling (Ng et al., 2004; Rüsch et al., 2001; Sharlin et al., 2018), P253L mice did not display any impairment in auditory functions using ABR. This is a positive feature for P253L mice as a model of MCT8 deficiency as it allows for different cognitive evaluations based

on auditory stimuli such as fear conditioning or eye-blink conditioning (Crawley, 2006), and it more accurately depicts AHDS symptomatology, which does not include deafness among its hallmarks.

P253L mice display very similar endocrine, brain histological and behavioral phenotype to *Mct8/Oatp1c1* KO (Mayerl et al., 2014)) and *Mct8/Dio2* KO mice (Bárez-López et al., 2019), with the advantage that in P253L there are no additional mutations in other proteins involved in TH metabolism. Altogether, these results indicate that the avatar P253L mouse model is a suitable mammalian model for the AHDS as it mimics the thyroidal profile, alterations in neuroarchitecture and the GABAergic system, presents motor skills and emotional alterations, and does not have auditory impairments due to mutations in MCT8.

In addition, the comparison between P253L and *Mct8* KO animals has revealed important findings that need to be considered. Even though most THs levels in blood and tissues are very similar between P253L and *Mct8* KO animals, P253L mice display histological and motor skill alterations that are not present in *Mct8* KO animals. This is even more puzzling taking into account that the expression of TH-target genes is impaired in *Mct8* KO but not in P253L. A few possibilities underlying these effects can be discussed. First, in this study, the THs profile and gene expression of TH-target genes were only explored at one time during development. Therefore, the histological and behavioral alterations found in P253L mice could be arising from TH content and TH-target gene expression impairments at earlier stages of development. Second, as P253L mice have reduced T4 brain content in comparison to *Mct8* KO mice, most probably due to the lack of increased *Oatp1c1*, it is possible that impairments in the local conversion of T4 into T3 at target brain areas or cell populations could be mediating the histological and behavioral alterations (Guadaño-Ferraz et al., 1997). Moreover, it is tempting to speculate that a reduction in T4 might be impairing potential T4 genomic and extra-genomic effects (Davis et al., 2016; Galton, 2017; Galton et al., 2007; Gil-Ibáñez et al., 2017). Finally, as additional pathophysiological mechanisms, the MCT8 P253L mutation could be resulting in a gain of toxic function at a cellular level or the generation of MCT8 with altered membrane mobility could be impairing the mobility and function of other membrane components, thus altering cellular homeostasis.

5. Conclusions

Several conclusions arise from this work: 1) MCT8 missense mutation P321L, leads to the generation of new interactions between residues, that eventually alter the protein structure, including the MCT8 substrate binding pocket, and finally prevent MCT8 transporting function. 2) P253L mice exhibit peripheral hyperthyroidism and brain hypothyroidism, both with a decrease in T3 and T4 levels, replicating the thyroid status observed in the patients of AHDS. 3) *Mct8* KO and P253L mice present similar TH levels in blood and tissues, with the exemption of T4 in cerebral cortex that is decreased in P253L but not in Mct8KO mice. 4) While the OATP1C1 transporter compensates for the lack of MCT8 in both *Mct8* KO and P253L mice, the expression of this transporter is lower in P253L mice than in *Mct8* KO mice, possibly leading to low T4 content in the cerebral cortex. 5) P253L mice present also severe alterations in brain histology, in general neuroarchitecture, and also in particular in the GABAergic system, which recapitulates one of the main hallmarks of the disease. 6) The neurohistological alterations observed on P253L mice translate into a motor and emotional phenotype, thus making it a suitable model of the disease.7) It is now feasible to produce an "avatar model" for a patient with AHDS within a few months, creating new opportunities to design and test therapeutic interventions.

Altogether, we conclude that further characterization of this murine model may be key to understanding the molecular basis of the pathological defects in MCT8 deficiency, whilst it offers a highly valuable tool to perform preclinical studies to test potential therapeutic options such as *in vivo* gene therapy (Iwayama et al., 2016; Liao et al., 2022; Sundaram et al., 2022) and precision medicine solutions to revert the devastating impairments in MCT8 deficiency.

Author contributions

VV-H, SB-L, AG-F conceived and planned the research studies. VV-H, MB-A, AG-A and MG-Y carried out the experiments. CG-M supervised the RIA assays performed by VV-H. FF and SM generated the mouse model and CG-M established the colony at our animal facility. VV-H and AM-P quantified the data and VV-H, MB-A, MG-Y, AM-P, SB-L and AG-F analyzed the data. AG-F supervised and administered the project. VV-H wrote the manuscript with support from SB-L and AG-F. All authors discussed the results and commented on the manuscript.

Funding

This study was supported by MCIN/AEI/10.13039/501100011033 (Grant No. SAF2017-86342-R to AG-F); MCIN/AEI/10.13039/501100011033/FEDER "Una manera de hacer Europa" (Grant No PID2020-113139RB-I00 to AG-F); Consejo Superior de Investigaciones Científicas (Grant No. 2020AEP044 to AG-F); the Sherman Foundation (Grant No. OTR02211 to SB-L and AG-F); Asociación Corriendo con el Corazón por Hugo (Grant No OTR06190 to AG-F) and the BBSRC (grant number BB/R016879/1 to SB-L). VV-H is recipient of a contract from MCIN/AEI /10.13039/501100011033/FSE "El FSE invierte en tu futuro" (Grant No PRE2018–086185), MG-Y and MB-A from the Formación de Profesorado Universitario (FPU, FPU19/02006 and FPU17/01733 respectively) program from the Ministerio de Ciencia, Innovación y Universidades.

CRediT authorship contribution statement

Víctor Valcárcel-Hernández: Conceptualization, Methodology, Validation, Formal analysis, Investigation, Data curation, Writing – original draft, Writing – review & editing, Visualization. **Marina Guillén-Yunta:** Formal analysis, Investigation, Writing – original draft, Writing – review & editing, Visualization. **Miranda Bueno-Arribas:** Methodology, Software, Formal analysis, Investigation, Resources, Writing – original draft, Writing – review & editing, Visualization. **Ana Montero-Pedrazuela:** Validation, Formal analysis, Data curation, Writing – review & editing. **Carmen Grijota-Martínez:** Investigation, Resources, Writing – review & editing. **Suzy Markossian:** Methodology, Resources. **Ángel García-Aldea:** Investigation, Writing – review & editing. **Frédéric Flamant:** Methodology, Resources, Writing – review & editing. **Soledad Bárez-López:** Conceptualization, Methodology, Validation, Formal analysis, Data curation, Writing – original draft, Writing – review & editing, Supervision, Funding acquisition. **Ana Guadaño-Ferraz:** Conceptualization, Methodology, Validation, Writing – original draft, Writing – review & editing, Supervision, Project administration, Funding acquisition.

Conflict of interest

The authors have declared that no conflict of interest exists.

Data availability

Data will be made available on request.

Acknowledgements

We thank Sabine Richard for her helpful comments on the manuscript. Also, we thank Olivier Vincent and Ricardo Escalante for kindly providing the software PyMOL (The PyMOL Molecular Graphics System, Version 2.4.0 Schrödinger, LLC) for testing. We would like to thank José Luis Trejo for his help with the behavioral analysis, the Genomics Core Facility at the IIBM and Silvia Murillo for her technical help and Coral

Pedrero and Cristina Crespo for their technical help and animal care. The graphical abstract was created thanks to http://Biorender.com and Servier Medical Art.

Appendix A. Supplementary data

Supplementary data to this article can be found online at https://doi.org/10.1016/j.nbd.2022.105896.

References

Allan, W., Herndon, C.N., Dudley, F.C., 1944. Some examples of the inheritance of mental deficiency: apparently sex-linked idiocy and microcephaly. Am. J. Ment. Defic. 48, 325–334.

Arqué, G., de Lagrán, M.M., Arbonés, M.L., Dierssen, M., 2009. Age-associated motor and visuo-spatial learning phenotype in Dyrk1A heterozygous mutant mice. Neurobiol. Dis. 36, 312–319. https://doi.org/10.1016/j.nbd.2009.07.027.

Baek, M., DiMaio, F., Anishchenko, I., Dauparas, J., Ovchinnikov, S., Lee, G.R., Wang, J., Cong, Q., Kinch, L.N., Dustin Schaeffer, R., Millán, C., Park, H., Adams, C., Glassman, C.R., DeGiovanni, A., Pereira, J.H., Rodrigues, A.V., Van Dijk, A.A., Ebrecht, A.C., Opperman, D.J., Sagmeister, T., Buhlheller, C., Pavkov-Keller, T., Rathinaswamy, M.K., Dalwadi, U., Yip, C.K., Burke, J.E., Christopher Garcia, K., Grishin, N.V., Adams, P.D., Read, R.J., Baker, D., 2021. Accurate prediction of protein structures and interactions using a three-track neural network. Science 373, 871–876. https://doi.org/10.1126/science.abj8754.

Bárez-López, S., Bosch-García, D., Gómez-Andrés, D., Pulido-Valdeolivas, I., Montero-Pedrazuela, A., Obregon, M.J., Guadaño-Ferraz, A., 2014. Abnormal motor phenotype at adult stages in mice lacking type 2 deiodinase. PLoS One 9. https://doi.org/10.1371/journal.pone.0103857.

Bárez-López, S., Montero-Pedrazuela, A., Bosch-García, D., Venero, C., Guadaño-Ferraz, A., 2017a. Increased anxiety and fear memory in adult mice lacking type 2 deiodinase. Psychoneuroendocrinology 84, 51–60. https://doi.org/10.1016/j.psyneuen.2017.06.013.

Bárez-López, S., Obregon, M.J., Bernal, J., Guadaño-Ferraz, A., 2017b. Thyroid hormone economy in the perinatal mouse brain: implications for cerebral cortex development. Cereb. Cortex 1–11. https://doi.org/10.1093/cercor/bhx088.

Bárez-López, S., Grijota-Martínez, C., Ausó, E., Fernández-De Frutos, M., Montero-Pedrazuela, A., Guadaño-Ferraz, A., 2019. Adult mice lacking Mct8 and Dio2 proteins present alterations in peripheral thyroid hormone levels and severe brain and motor skill impairments. Thyroid 29, 1669–1682. https://doi.org/10.1089/thy.2019.0068.

Bernal, J., Guadaño-Ferraz, A., Morte, B., 2015. Thyroid hormone transporters—functions and clinical implications. Nat. Rev. Endocrinol. 11, 406. https://doi.org/10.1038/nrendo.2015.66.

Bowie, J.U., Ltcy, R., Eisenberg, D., 1991. A method to identify protein sequences that fold into a known three-dimensional stucture, 253 (5016), 164–170.

Braun, D., Bohleber, S., Vatine, G.D., Svendsen, C.N., Schweizer, U., 2022. Sodium phenylbutyrate rescues thyroid hormone transport in brain endothelial-like cells. Thyroid 1–31. https://doi.org/10.1089/thy.2021.0643.

Ceballos, A., Belinchon, M.M., Sanchez-Mendoza, E., Grijota-Martinez, C., Dumitrescu, A. M., Refetoff, S., Morte, B., Bernal, J., 2009. Importance of monocarboxylate transporter 8 for the blood-brain barrier-dependent availability of 3,5,3′-triiodo-L-thyronine. Endocrinology 150, 2491–2496. https://doi.org/10.1210/en.2008-1616.

Cediel, R., Riquelme, R., Contreras, J., Díaz, A., Varela-Nieto, I., 2006. Sensorineural hearing loss in insulin-like growth factor I-null mice: a new model of human deafness. Eur. J. Neurosci. 23, 587–590. https://doi.org/10.1111/j.1460-9568.2005.04584.x.

Colovos, C., Yeates, T.O., 1993. Verification of protein structures: patterns of nonbonded atomic interactions. Protein Sci. 2, 1511–1519. https://doi.org/10.1002/pro.5560020916.

Crawley, J., 2006. What's Wrong with my Mouse?: Behavioral Phenotyping of Transgenic and Knockout Mice, Second edition, pp. 1–523. https://doi.org/10.1002/9780470119051.

Davis, P.J., Goglia, F., Leonard, J.L., 2016. Nongenomic actions of thyroid hormone. Nat. Rev. Endocrinol. 12, 111–121. https://doi.org/10.1038/nrendo.2015.205.

DeFelipe, J., 1999. Chandelier cells and epilepsy. Brain 122, 1807–1822. https://doi.org/10.1093/brain/122.10.1807.

Dumitrescu, A.M., Liao, X.-H., Best, T.B., Brockmann, K., Refetoff, S., 2004. A novel syndrome combining thyroid and neurological abnormalities is associated with mutations in a monocarboxylate transporter gene. Am. J. Hum. Genet. 74, 168–175. https://doi.org/10.1086/380999.

Dumitrescu, A.M., Liao, X., Weiss, R.E., Millen, K., Refetoff, S., 2006. Tissue-specific thyroid hormone deprivation and excess in monocarboxylate transporter (Mct) 8-deficient mice. Endocrinology 147, 4036–4043. https://doi.org/10.1210/en.2006-0390.

Friesema, E.C.H., Ganguly, S., Abdalla, A., Manning Fox, J.E., Halestrap, A.P., Visser, T. J., 2003. Identification of monocarboxylate transporter 8 as a specific thyroid hormone transporter. J. Biol. Chem. 278, 40128–40135. https://doi.org/10.1074/jbc.M300909200.

Friesema, E.C.H., Grueters, A., Biebermann, H., Krude, H., von Moers, A., Reeser, M., Barrett, T.G., Mancilla, E.E., Svensson, J., Kester, M.H.A., Kuiper, G.G.J.M., Balkassmi, S., Uitterlinden, A.G., Koehrle, J., Rodien, P., Halestrap, A.P., Visser, T.J., 2004. Association between mutations in a thyroid hormone transporter and severe X-linked psychomotor retardation. Lancet (London, England) 364, 1435–1437. https://doi.org/10.1016/S0140-6736(04)17226-7.

Gagliardi, L., Nataren, N., Feng, J., Schreiber, A.W., Hahn, C.N., Conwell, L.S., Coman, D., Scott, H.S., 2015. Allan-Herndon-Dudley syndrome with unusual profound sensorineural hearing loss. Am. J. Med. Genet. Part A 167, 1872–1876. https://doi.org/10.1002/ajmg.a.37075.

Galton, V.A., 2017. The ups and downs of the thyroxine pro-hormone hypothesis. Mol. Cell. Endocrinol. 458, 105–111. https://doi.org/10.1016/j.mce.2017.01.029.

Galton, V.A., Wood, E.T., St. Germain, E.A., Withrow, C.A., Aldrich, G., St. Germain, G. M., Clark, A.S., St. Germain, D.L., 2007. Thyroid hormone homeostasis and action in the type 2 deiodinase-deficient rodent brain during development. Endocrinology 148, 3080–3088. https://doi.org/10.1210/en.2006-1727.

Gilbert, M.E., Lasley, S.M., 2013. Developmental thyroid hormone insufficiency and brain development: a role for brain-derived neurotrophic factor (BDNF)? Neuroscience. https://doi.org/10.1016/j.neuroscience.2012.11.022.

Gilbert, M.E., Sui, L., Walker, M.J., Anderson, W., Thomas, S., Smoller, S.N., Schon, J.P., Phani, S., Goodman, J.H., 2007. Thyroid hormone insufficiency during brain development reduces parvalbumin immunoreactivity and inhibitory function in the hippocampus. Endocrinology 148, 92–102. https://doi.org/10.1210/en.2006-0164.

Gil-Ibáñez, P., Belinchón, M.M., Morte, B., Obregón, M.J., Bernal, J., 2017. Is the intrinsic genomic activity of thyroxine relevant in vivo? Effects on gene expression in primary cerebrocortical and neuroblastoma cells. Thyroid 27, 1092–1098. https://doi.org/10.1089/thy.2017.0024.

Grijota-Martínez, C., Bárez-López, S., Gómez-Andrés, D., Guadaño-Ferraz, A., 2020. MCT8 deficiency: the road to therapies for a rare disease. Front. Neurosci. 14, 1–8. https://doi.org/10.3389/fnins.2020.00380.

Groeneweg, S., Kersseboom, S., Van Den Berge, A., Dolcetta-Capuzzo, A., Van Geest, F.S., Van Heerebeek, R.E.A., Arjona, F.J., Meima, M.E., Peeters, R.P., Visser, W.E., Visser, T.J., 2019a. In vitro characterization of human, mouse, and zebrafish MCT8 orthologues. Thyroid 29, 1499–1510. https://doi.org/10.1089/thy.2019.0009.

Groeneweg, S., van Geest, F.S., Peeters, R.P., Heuer, H., Visser, W.E., 2019b. Thyroid hormone transporters. Endocr. Rev. 41, 146–201. https://doi.org/10.1210/endrev/bnz008.

Groeneweg, S., van Geest, F.S., Abacı, A., Alcantud, A., Ambegaonkar, G.P., Armour, C. M., Bakhtiani, P., Barca, D., Bertini, E.S., van Beynum, I.M., Brunetti-Pierri, N., Bugiani, M., Cappa, M., Cappuccio, G., Castellotti, B., Castiglioni, C., Chatterjee, K., de Coo, I.F.M., Coutant, R., Craiu, D., Crock, P., DeGoede, C., Demir, K., Dica, A., Dimitri, P., Dolcetta-Capuzzo, A., Dremmen, M.H.G., Dubey, R., Enderli, A., Fairchild, J., Gallichan, J., George, B., Gevers, E.F., Hackenberg, A., Halász, Z., Heinrich, B., Huynh, T., Kłosowska, A., van der Knaap, M.S., van der Knoop, M.M., Konrad, D., Koolen, D.A., Krude, H., Lawson-Yuen, A., Lebl, J., Linder-Lucht, M., Lorea, C.F., Lourenço, C.M., Lunsing, R.J., Lyons, G., Malikova, J., Mancilla, E.E., McGowan, A., Mericq, V., Lora, F.M., Moran, C., Müller, K.E., Oliver-Petit, I., Paone, L., Paul, P.G., Polak, M., Porta, F., Poswar, F.O., Reinauer, C., Rozenkova, K., Menevse, T.S., Simm, P., Simon, A., Singh, Y., Spada, M., van der Spek, J., Stals, M.A. M., Stoupa, A., Subramanian, G.M., Tonduti, D., Turan, S., den Uil, C.A., Vanderniet, J., van der Walt, A., Wémeau, J.L., Wierzba, J., de Wit, M.C.Y., Wolf, N. I., Wurm, M., Zibordi, F., Zung, A., Zwaveling-Soonawala, N., Visser, W.E., 2020. Disease characteristics of MCT8 deficiency: an international, retrospective, multicentre cohort study. Lancet Diabetes Endocrinol. 8, 594–605. https://doi.org/10.1016/S2213-8587(20)30153-4.

Guadaño-Ferraz, A., Obregón, M.J., St Germain, D.L., Bernal, J., Obregon, M.J., StGermain, D.L., 1997. The type 2 iodothyronine deiodinase is expressed primarily in glial cells in the neonatal rat brain. Proc. Natl. Acad. Sci. U. S. A. 94, 10391–10396. https://doi.org/10.1073/pnas.94.19.10391.

Hadjab-Lallemend, S., Wallis, K., van Hogerlinden, M., Dudazy, S., Nordström, K., Vennström, B., Fisahn, A., 2010. A mutant thyroid hormone receptor alpha1 alters hippocampal circuitry and reduces seizure susceptibility in mice. Neuropharmacology 58, 1130–1139. https://doi.org/10.1016/j.neuropharm.2010.02.005.

Hébert, R., Langlois, J.M., Dussault, J.H., 1985. Permanent defects in rat peripheral auditory function following perinatal hypothyroidism: determination of a critical period. Dev. Brain Res. 23, 161–170. https://doi.org/10.1016/0165-3806(85)90037-9.

Iwayama, H., Liao, X.-H., Braun, L., Bárez-López, S., Kaspar, B., Weiss, R.E., Dumitrescu, A.M., Guadaño-Ferraz, A., Refetoff, S., 2016. Adeno associated virus 9–based gene therapy delivers a functional monocarboxylate transporter 8, improving thyroid hormone availability to the brain of Mct8-deficient mice. Thyroid 26, 1311–1319. https://doi.org/10.1089/thy.2016.0060.

Kaila, K., Ruusuvuori, E., Seja, P., Voipio, J., Puskarjov, M., 2014. GABA actions and ionic plasticity in epilepsy. Curr. Opin. Neurobiol. 26, 34–41. https://doi.org/10.1016/j.conb.2013.11.004.

Kersseboom, S., Kremers, G.J., Friesema, E.C.H., Edward Visser, W., Klootwijk, W., Peeters, R.P., Visser, T.J., 2013. Mutations in MCT8 in patients with Allan-Herndon-Dudley-syndrome affecting its cellular distribution. Mol. Endocrinol. 27, 801–813. https://doi.org/10.1210/me.2012-1356.

Kinne, A., Kleinau, G., Hoefig, C.S., Grüters, A., Köhrle, J., Krause, G., Schweizer, U., 2010. Essential molecular determinants for thyroid hormone transport and first structural implications for monocarboxylate transporter 8. J. Biol. Chem. 285, 28054–28063. https://doi.org/10.1074/jbc.M110.129577.

Kleinau, G., Schweizer, U., Kinne, A., Köhrle, J., Grüters, A., Krude, H., Biebermann, H., 2011. Insights into molecular properties of the human monocarboxylate transporter 8 by combining functional with structural information. Thyroid. Res. 4, S4. https://doi.org/10.1186/1756-6614-4-S1-S4.

Laskowski, R.A., Rullmann, J.A.C., MacArthur, M.W., Kaptein, R., Thornton, J.M., 1996. AQUA and PROCHECK-NMR: programs for checking the quality of protein structures solved by NMR. J. Biomol. NMR 8, 477–486. https://doi.org/10.1007/BF00228148.

Lehmann, K., Steinecke, A., Bolz, J., 2012. GABA through the ages: regulation of cortical function and plasticity by inhibitory interneurons. Neural Plast. 2012 https://doi.org/10.1155/2012/892784.

Li, Z., Jaroszewski, L., Iyer, M., Sedova, M., Godzik, A., 2020. FATCAT 2.0: towards a better understanding of the structural diversity of proteins. Nucleic Acids Res. 48, W60–W64. https://doi.org/10.1093/NAR/GKAA443.

Liao, X.-H., Avalos, P., Shelest, O., Ofan, R., Shilo, M., Bresee, C., Likhite, S., Vit, J.-P., Heuer, H., Kaspar, B., Meyer, K., Dumitrescu, A.M., Refetoff, S., Svendsen, C.N., Vatine, G.D., 2022. AAV9-MCT8 delivery at juvenile stage ameliorates neurological and behavioral deficits in a mouse model of MCT8-deficiency. Thyroid 32, 849–859. https://doi.org/10.1089/thy.2022.0034.

Lister, R.G., 1987. The use of a plus-maze to measure anxiety in the mouse. Psychopharmacology 92, 180–185. https://doi.org/10.1007/BF00177912.

López-Espíndola, D., Morales-Bastos, C., Grijota-Martínez, C., Liao, X.-H., Lev, D., Sugo, E., Verge, C.F., Refetoff, S., Bernal, J., Guadaño-Ferraz, A., 2014. Mutations of the thyroid hormone transporter MCT8 cause prenatal brain damage and persistent hypomyelination. J. Clin. Endocrinol. Metab. 99, E2799–E2804. https://doi.org/10.1210/jc.2014-2162.

Martin, A.J.M., Vidotto, M., Boscariol, F., Di Domenico, T., Walsh, I., Tosatto, S.C.E., 2011. RING: networking interacting residues, evolutionary information and energetics in protein structures. Bioinformatics 27, 2003–2005. https://doi.org/10.1093/bioinformatics/btr191.

Masnada, S., Sarret, C., Antonello, C.E., Fadilah, A., Krude, H., Mura, E., Mordekar, S., Nicita, F., Olivotto, S., Orcesi, S., Porta, F., Remerand, G., Siri, B., Wilpert, N.M., Amir-Yazdani, P., Bertini, E., Schuelke, M., Bernard, G., Boespflug-Tanguy, O., Tonduti, D., 2022. Movement disorders in MCT8 deficiency/Allan-Herndon-Dudley syndrome. Mol. Genet. Metab. 135, 109–113. https://doi.org/10.1016/j.ymgme.2021.12.003.

Matheus, M.G., Lehman, R.K., Bonilha, L., Holden, K.R., 2015. Redefining the pediatric phenotype of X-linked monocarboxylate transporter 8 (MCT8) deficiency: implications for diagnosis and therapies. J. Child Neurol. 30, 1664–1668. https://doi.org/10.1177/0883073815578524.

Mayerl, S., Müller, J., Bauer, R., Richert, S., Kassmann, C.M., Darras, V.M., Buder, K., Boelen, A., Visser, T.J., Heuer, H., 2014. Transporters MCT8 and OATP1C1 maintain murine brain thyroid hormone homeostasis. J. Clin. Invest. 124, 1987–1999. https://doi.org/10.1172/JCI70324.

Mayerl, S., Martin, A.A., Bauer, R., Schwaninger, M., Heuer, H., Ffrench-Constant, C., 2022. Distinct actions of the thyroid hormone transporters McT8 and Oatp1c1 in murine adult hippocampal neurogenesis. Cells 11, 1–15. https://doi.org/10.3390/cells11030524.

Morreale de Escobar, G., Pastor, R., Obregon, M.J., Escobar del Rey, F., 1985. Effects of maternal hypothyroidism on the weight and thyroid hormone content of rat embryonic tissues, before and after onset of fetal thyroid function. Endocrinology 117, 1890–1900. https://doi.org/10.1210/endo-117-5-1890.

Morte, B., Ceballos, A., Diez, D., Grijota-Martínez, C., Dumitrescu, A.M., Di Cosmo, C., Galton, V.A., Refetoff, S., Bernal, J., 2010a. Thyroid hormone-regulated mouse cerebral cortex genes are differentially dependent on the source of the hormone: a study in monocarboxylate transporter-8- and deiodinase-2-deficient mice. Endocrinology 151, 2381–2387. https://doi.org/10.1210/en.2009-0944.

Morte, B., Ceballos, A., Diez, D., Grijota-Martínez, C., Dumitrescu, A.M., Di Cosmo, C., Galton, V.A., Refetoff, S., Bernal, J., 2010b. Thyroid hormone-regulated mouse cerebral cortex genes are differentially dependent on the source of the hormone: a study in monocarboxylate transporter-8- and deiodinase-2-deficient mice. Endocrinology 151, 2381–2387. https://doi.org/10.1210/en.2009-0944.

Ng, L., Goodyear, R.J., Woods, C.A., Schneider, M.J., Diamond, E., Richardson, G.P., Kelley, M.W., St. Germain, D.L., Galton, V.A., Forrest, D., 2004. Hearing loss and retarded cochlear development in mice lacking type 2 iodothyronine deiodinase. Proc. Natl. Acad. Sci. U. S. A. 101, 3474–3479. https://doi.org/10.1073/pnas.0307402101.

Obregon, M.J., Morreale de Escobar, G., Escobar del Rey, F., 1978. Concentrations of triiodo-L-thyronine in the plasma and tissues of normal rats, as determined by radioimmunoassay: comparison with results obtained by an isotopic equilibrium technique*. Endocrinology 103, 2145–2153. https://doi.org/10.1210/endo-103-6-2145.

Paxinos, G., Franklin, K.B.J., 2004. The Mouse Brain in Stereotaxic Coordinates. Elsevier Academic Press.

Piovesan, D., Minervini, G., Tosatto, S.C.E., 2016. The RING 2.0 web server for high quality residue interaction networks. Nucleic Acids Res. 44, W367–W374. https://doi.org/10.1093/nar/gkw315.

Refetoff, S., Pappa, T., Williams, M.K., Matheus, M.G., Liao, X.H., Hansen, K., Nicol, L., Pierce, M., Blasco, P.A., Jensen, M.W., Bernal, J., Weiss, R.E., Dumitrescu, A.M., Lafranchi, S., 2021. Prenatal treatment of thyroid hormone cell membrane transport defect caused by MCT8 gene mutation. Thyroid 31, 713–720. https://doi.org/10.1089/thy.2020.0306.

Remerand, G., Boespflug-Tanguy, O., Tonduti, D., Touraine, R., Rodriguez, D., Curie, A., Perreton, N., Des Portes, V., Sarret, C., Afenjar, A., Burglen, L., Castellotti, B., Cuntz, D., Desguerre, I., Doummar, D., Estienne, M., Freri, E., Heron, D., Moutard, M. L., Novara, F., Orcesi, S., Saletti, V., Zibordi, F., 2019. Expanding the phenotypic spectrum of Allan–Herndon–Dudley syndrome in patients with SLC16A2 mutations. Dev. Med. Child Neurol. 61, 1439–1447. https://doi.org/10.1111/dmcn.14332.

Richard, S., Aguilera, N., Thévenet, M., Dkhissi-Benyahya, O., Flamant, F., 2017. Neuronal expression of a thyroid hormone receptor α mutation alters mouse behaviour. Behav. Brain Res. 321, 18–27. https://doi.org/10.1016/j.bbr.2016.12.025.

Ruiz de Oña, C., Obregón, M.J., Escobar del Rey, F., Morreale de Escobar, G., 1988. Developmental changes in rat brain 5′-deiodinase and thyroid hormones during the fetal period: the effects of fetal hypothyroidism and maternal thyroid hormones. Pediatr. Res. 24, 588–594. https://doi.org/10.1203/00006450-198811000-00010.

Rüsch, A., Ng, L., Goodyear, R., Oliver, D., Lisoukov, I., Vennström, B., Richardson, G., Kelley, M.W., Forrest, D., 2001. Retardation of cochlear maturation and impaired hair cell function caused by deletion of all known thyroid hormone receptors. J. Neurosci. 21, 9792–9800. https://doi.org/10.1523/jneurosci.21-24-09792.2001.

Sarret, C., Oliver Petit, I., Tonduti, D., 2022. Allan-Herndon-Dudley Syndrome. GeneReviews® Seattle Univ. Washington, Seattle. n.d.

Schwartz, C.E., Stevenson, R.E., 2007. The MCT8 thyroid hormone transporter and Allan-Herndon-Dudley syndrome. Best Pract. Res. Clin. Endocrinol. Metab. 21, 307–321. https://doi.org/10.1016/j.beem.2007.03.009.

Schweizer, U., Johannes, J., Bayer, D., Braun, D., 2014. Structure and function of thyroid hormone plasma membrane transporters. Eur. Thyroid J. 3, 143–153. https://doi.org/10.1159/000367858.

Sharlin, D.S., Ng, L., Verrey, F., Visser, T.J., Liu, Y., Olszewski, R.T., Hoa, M., Heuer, H., Forrest, D., 2018. Deafness and loss of cochlear hair cells in the absence of thyroid hormone transporters Slc16a2 (Mct8) and Slc16a10 (Mct10). Sci. Rep. 8, 1–14. https://doi.org/10.1038/s41598-018-22553-w.

Sievers, F., Higgins, D.G., 2018. Clustal omega for making accurate alignments of many protein sequences. Protein Sci. 27, 135–145. https://doi.org/10.1002/pro.3290.

Strømme, P., Groeneweg, S., Lima de Souza, E.C., Zevenbergen, C., Torgersbråten, A., Holmgren, A., Gurcan, E., Meima, M.E., Peeters, R.P., Visser, W.E., Høneren Johansson, L., Babovic, A., Zetterberg, H., Heuer, H., Frengen, E., Misceo, D., Visser, T.J., 2018. Mutated thyroid hormone transporter OATP1C1 associates with severe brain hypometabolism and juvenile neurodegeneration. Thyroid 28, 1406–1415. https://doi.org/10.1089/thy.2018.0595.

Sundaram, S.M., Arrulo Pereira, A., Müller-Fielitz, H., Köpke, H., De Angelis, M., Müller, T.D., Heuer, H., Körbelin, J., Krohn, M., Mittag, J., Nogueiras, R., Prevot, V., Schwaninger, M., 2022. Gene therapy targeting the blood-brain barrier improves neurological symptoms in a model of genetic MCT8 deficiency. Brain. https://doi.org/10.1093/brain/awac243.

Tamijani, S.M.S., Karimi, B., Amini, E., Golpich, M., Dargahi, L., Ali, R.A., Ibrahim, N.M., Mohamed, Z., Ghasemi, R., Ahmadiani, A., 2015. Thyroid hormones: possible roles in epilepsy pathology. Seizure 31, 155–164. https://doi.org/10.1016/j.seizure.2015.07.021.

Tapias, V., Greenamyre, J.T., Watkins, S.C., 2013. Automated imaging system for fast quantitation of neurons, cell morphology and neurite morphometry in vivo and in vitro. Neurobiol. Dis. 54, 158–168. https://doi.org/10.1016/j.nbd.2012.11.018. Automated.

Teixeira, M., Py, B.F., Bosc, C., Laubreton, D., Moutin, M.J., Marvel, J., Flamant, F., Markossian, S., 2018. Electroporation of mice zygotes with dual guide RNA/Cas9 complexes for simple and efficient cloning-free genome editing. Sci. Rep. 8, 1–9. https://doi.org/10.1038/s41598-017-18826-5.

Tian, W., Chen, C., Lei, X., Zhao, J., Liang, J., 2018. CASTp 3.0: computed atlas of surface topography of proteins. Nucleic Acids Res. 46, W363–W367. https://doi.org/10.1093/nar/gky473.

Trajkovic, M., Visser, T.J., Mittag, J., Horn, S., Lukas, J., Darras, V.M., Raivich, G., Bauer, K., Heuer, H., 2007. Abnormal thyroid hormone metabolism in mice lacking the monocarboxylate transporter 8. J. Clin. Invest. 117, 627–635. https://doi.org/10.1172/JCI28253.A.

Tunyasuvunakool, K., Adler, J., Wu, Z., Green, T., Zielinski, M., Žídek, A., Bridgland, A., Cowie, A., Meyer, C., Laydon, A., Velankar, S., Kleywegt, G.J., Bateman, A., Evans, R., Pritzel, A., Figurnov, M., Ronneberger, O., Bates, R., Kohl, S.A.A., Potapenko, A., Ballard, A.J., Romera-Paredes, B., Nikolov, S., Jain, R., Clancy, E., Reiman, D., Petersen, S., Senior, A.W., Kavukcuoglu, K., Birney, E., Kohli, P., Jumper, J., Hassabis, D., 2021. Highly accurate protein structure prediction for the human proteome. Nature 596, 590–596. https://doi.org/10.1038/s41586-021-03828-1.

Valcárcel-Hernández, V., López-Espíndola, D., Guillén-Yunta, M., García-Aldea, Á., de Toledo, López, Soler, I., Bárez-López, S., Guadaño-Ferraz, A., 2022. Deficient thyroid hormone transport to the brain leads to impairments in axonal caliber and oligodendroglial development. Neurobiol. Dis. 162 https://doi.org/10.1016/j.nbd.2021.105567.

Vatine, G.D., Al-Ahmad, A., Barriga, B.K., Svendsen, S., Salim, A., Garcia, L., Garcia, V.J., Ho, R., Yucer, N., Qian, T., Lim, R.G., Wu, J., Thompson, L.M., Spivia, W.R., Chen, Z., Van Eyk, J., Palecek, S.P., Refetoff, S., Shusta, E.V., Svendsen, C.N., 2017. Modeling psychomotor retardation using iPSCs from MCT8-deficient patients indicates a prominent role for the blood-brain barrier. Cell Stem Cell 20, 831–843.e5. https://doi.org/10.1016/j.stem.2017.04.002.

Vatine, G.D., Barrile, R., Workman, M.J., Sances, S., Barriga, B.K., Rahnama, M., Barthakur, S., Kasendra, M., Lucchesi, C., Kerns, J., Wen, N., Spivia, W.R., Chen, Z., Van Eyk, J., Svendsen, C.N., 2019. Human iPSC-derived blood-brain barrier chips enable disease modeling and personalized medicine applications. Cell Stem Cell 24, 995–1005.e6. https://doi.org/10.1016/j.stem.2019.05.011.

Vaurs-Barrière, C., Deville, M., Sarret, C., Giraud, G., Des Portes, V., Prats-Viñas, J.M., De Michele, G., Dan, B., Brady, A.F., Boespflug-Tanguy, O., Touraine, R., 2009. Pelizaeus-merzbacher-like disease presentation of MCT8 mutated male subjects. Ann. Neurol. 65, 114–118. https://doi.org/10.1002/ana.21579.

Venero, C., Guadaño-Ferraz, A., Herrero, A.I., Nordström, K., Manzano, J., De Escobar, G. M., Bernal, J., Vennström, B., 2005. Anxiety, memory impairment, and locomotor dysfunction caused by a mutant thyroid hormone receptor ??1 can be ameliorated by T3 treatment. Genes Dev. 19, 2152–2163. https://doi.org/10.1101/gad.346105.

Verge, C.F., Konrad, D., Cohen, M., Di Cosmo, C., Dumitrescu, A.M., Marcinkowski, T., Hameed, S., Hamilton, J., Weiss, R.E., Refetoff, S., 2012. Diiodothyropropionic acid (DITPA) in the treatment of MCT8 deficiency. J. Clin. Endocrinol. Metab. 97, 4515–4523. https://doi.org/10.1210/jc.2012-2556.

Wallis, K., Sjögren, M., van Hogerlinden, M., Silberberg, G., Fisahn, A., Nordström, K., Larsson, L., Westerblad, H., Morreale de Escobar, G., Shupliakov, O., Vennström, B., 2008. Locomotor deficiencies and aberrant development of subtype-specific GABAergic interneurons caused by an unliganded thyroid hormone receptor alpha1. J. Neurosci. 28, 1904–1915. https://doi.org/10.1523/JNEUROSCI.5163-07.2008.

Wang, N., Jiang, X., Zhang, S., Zhu, A., Yuan, Y., Xu, H., Lei, J., Yan, C., 2021. Structural basis of human monocarboxylate transporter 1 inhibition by anti-cancer drug candidates. Cell 184, 370–383.e13. https://doi.org/10.1016/j.cell.2020.11.043.

Weeke, J., Örskov, H., 1973. Synthesis of 125I monolabelled 3, 5, 3′-triiodothyronine and thyroxine of maximum specific activity for radioimmunoassay. Scand. J. Clin. Lab. Invest. 32, 357–360. https://doi.org/10.3109/00365517309084359.

Westholm, D.E., Salo, D.R., Viken, K.J., Rumbley, J.N., Anderson, G.W., 2009. The blood-brain barrier thyroxine transporter organic anion-transporting polypeptide 1c1 displays atypical transport kinetics. Endocrinology 150, 5153–5162. https://doi.org/10.1210/en.2009-0769.

Wirth, E.K., Roth, S., Blechschmidt, C., Hölter, S.M., Becker, L., Racz, I., Zimmer, A., Klopstock, T., Gailus-Durner, V., Fuchs, H., Wurst, W., Naumann, T., Bräuer, A., De Angelis, M.H., Köhrle, J., Grüters, A., Schweizer, U., 2009. Neuronal 3′,3,5-triiodothyronine (T3) uptake and behavioral phenotype of mice deficient in Mct8, the neuronal T3 transporter mutated in Allan-Herndon-Dudley syndrome. J. Neurosci. 29, 9439–9449. https://doi.org/10.1523/JNEUROSCI.6055-08.2009.

Ye, Y., Godzik, A., 2003. Flexible structure alignment by chaining aligned fragment pairs allowing twists. Bioinformatics 19. https://doi.org/10.1093/bioinformatics/btg1086.

Yin, Z., Burger, N., Kula-Alwar, D., Aksentijević, D., Bridges, H.R., Prag, H.A., Grba, D.N., Viscomi, C., James, A.M., Mottahedin, A., Krieg, T., Murphy, M.P., Hirst, J., 2021. Structural basis for a complex I mutation that blocks pathological ROS production. Nat. Commun. 12, 1–12. https://doi.org/10.1038/s41467-021-20942-w.

Zada, D., Tovin, A., Lerer-Goldshtein, T., Vatine, G.D., Appelbaum, L., 2014. Altered behavioral performance and live imaging of circuit-specific neural deficiencies in a zebrafish model for psychomotor retardation. PLoS Genet. 10 https://doi.org/10.1371/journal.pgen.1004615.

Zhang, B., Jin, Q., Xu, L., Li, N., Meng, Y., Chang, S., Zheng, X., Wang, J., Chen, Y., Neculai, D., Gao, N., Zhang, X., Yang, F., Guo, J., Ye, S., 2020. Cooperative transport mechanism of human monocarboxylate transporter 2. Nat. Commun. 11, 1–10. https://doi.org/10.1038/s41467-020-16334-1.